**Supporting Information**

# Acceleration and Regioselectivity Switching in 1,3-Dipolar Cycloaddition Reactions Confined in A Bis-Calix[4]pyrrole Cage

Yifan Li, Gemma Aragay, Pablo Ballester*

## CONTENTS

1. General information and instruments ..... S2
2. Synthesis and characterization data. ..... S3
2.1. Synthesis of 1-(2-propynyl)-4-pyridinone **4** ..... S3
2.2. Synthesis of 1,4-disubstituted 1,2,3-triazole pyridyl *N*-oxide derivatives. ..... S4
2.3. Synthesis of 1,5-disubstituted 1,2,3-triazole pyridine-*N*-oxide derivatives. ..... S12
3. Binding studies and characterization of octa-imine cage 1 with monotopic 1-(2-propynyl)-4-pyridinone **4** and disubstituted 1,2,3-triazole derivatives **7** and **8** in $CDCl_3$: $CD_3CN$ 9:1 mixture. . ..... S20
3.1. Binding studies of 1-(2-propynyl)-4-pyridinone **4** with **1**. ..... S20
3.2. Co-inclusion of 4-azido pyridine-*N*-oxide **2a** and 1-(2-propynyl)-4-pyridinone **4** in **1**. ..... S21
3.3. Co-inclusion of 4-azido(methyl) pyridine-*N*-oxide **2b** and 1-(2-propynyl)-4-pyridinone **4** in **1**. ..... S26
3.4. Co-inclusion of 4-azido(ethyl) pyridine-*N*-oxide **2c** and 1-(2-propynyl)-4-pyridinone **4** in **1**. ..... S36
4. Kinetic characterization of cycloaddition reaction ..... S49
4.1. Cycloaddition reactions of **2a-2c** with **4** in octa-imine cage **1**. ..... S49
4.2. Cycloaddition reactions of **2a-2b** with **4** in the bulk. ..... S51
5. References ..... S60

## 1. General information and instruments

Reagents were purchased from commercial suppliers and used without further purification. All reactions were performed under Ar atmosphere unless otherwise specified. All solvents were of HPLC grade quality, commercially obtained, and used without further purification except pyrrole, which was distilled and freshly used. Anhydrous solvents were obtained from a solvent purification system SPS-400-6 from Innovative Technologies.

Routine $^{1}$H NMR and $^{13}$C{$^{1}$H}NMR spectra were recorded on a Bruker Avance 400 (400 MHz for $^{1}$H NMR and 100 MHz for $^{13}$C NMR), Bruker Avance 500 (500 MHz for $^{1}$H NMR and 125 MHz for $^{13}$C NMR). Deuterated solvents (Eurisotop) are indicated in the characterization, and chemical shifts are given in ppm. Residual solvent peaks were used as references. All NMR *J* values are given in Hz. COSY, NOESY, and ROESY experiments were recorded to help with the proton assignment.

Mass spectrometry experiments were performed on a HPLC-MS-TOF (MicroTOF II, Bruker Daltonics). All ions were generated by electrospray ionization (ESI) in the positive and negative modes.

ITC experiments were performed in a MicroCal VP-ITC MicroCalorimeter using the VP Viewer 2000 software. All the titrations were carried out in chloroform: acetonitrile 9:1 solution mixture at 288 K. Titrations for monotopic guests were carried out by adding small aliquots (8 μL, 16 s) of a solution of guest into a solution of the host in the same solvent mixture. The spacing time between injections was set to 600 s. The concentration of the guest solution was approximately sixteen times more concentrated than the host solution. The association constants and the thermodynamic parameters were obtained from the fit of the titration data to the "two sets of sites" binding model implemented in the Microcal ITC Data Analysis software. For ditopic guests (**7a**, **7b** and **8b**), titrations were carried out by adding small aliquots of a solution of the host (~3 mM) into a solution of the guest (~0.3-0.6 mM) in the same solvent mixture. The association constants and the thermodynamic parameters were obtained from the fit of the titration data to the "one set of sites" binding model implemented in the Microcal ITC Data Analysis software.

HPLC analysis were performed using an Agilent technologies 1200 series equipped with a BEH HILIC column (3.5 μm, 4.6×150 mm, Waters Xbridge®) with the corresponding precolumn (3.5 μm, 3.9 mm × 5mm, Waters Xbridge®) and a gradient elution (from $CH_3CN/H_2O$ 98:2 to 60:40 in 15 min, 1 mL/min; Injection volume: 5 μL. Detection wavelength 300 and 276 nm).

## 2. Synthesis and characterization data.

Octa-imine cage **1**, monotopic pyridine *N*-oxides **2a**, **2b**, and **2b** were synthesized using reported procedures.[1] 1-(2-propynyl)-4-pyridinone **4** was synthesized by modifying the reported alkylation of 4-hydroxypyridine procedure in the literature.[2]

### 2.1. Synthesis of 1-(2-propynyl)-4-pyridinone 4

Under Ar, propargyl bromide (1.60 g, 11.0 mmol, 1.1 mL, 1 equiv.) was added to a suspension of 4-hydroxypyridine (1.00 g, 11.0 mmol, 1 equiv.), and $K_2CO_3$ (3.04 g, 22.0 mmol, 2 equiv.) in acetonitrile (50 mL). The reaction mixture was then refluxed at 80 ºC for 12 h. The reaction was monitored by TLC. After 12 h the resulting suspension was filtered, and the filtrate was evaporated under vacuum. The crude reaction mixture was purified by column chromatography (neutral alumina, DCM:isopropyl alcohol 97:3) to provide product **4** as a white solid in 80% yield (8.80 mmol, 1.10 g).

$^1$H NMR (400 MHz, 298 K, $CD_2Cl_2$): δ (ppm) = 7.44 (d, *J* = 7.8 Hz, 2H), 6.28 (d, *J* = 7.8 Hz, 2H), 4.60 (d, *J* = 2.6 Hz, 2H), 2.73 (t, *J*= 2.6 Hz, 1H). $^{13}$C{$^1$H} NMR (100 MHz, 298K, $CD_2Cl_2$): δ (ppm) =178.3, 139.1, 118.6, 76.4, 75.8, 45.3. HR-MS (ESI TOF) m/z: $[M+H]^+$ calculated for $C_8H_8NO^+$ = 134.0600, found 134.0603.

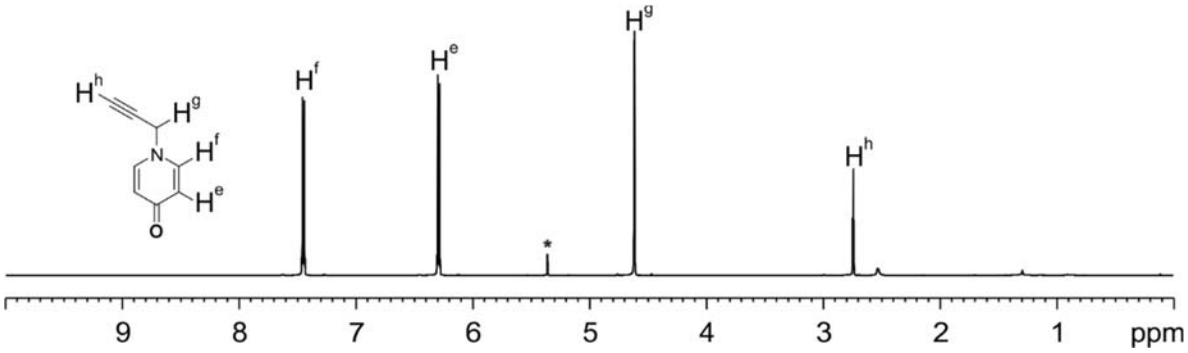


**Figure S 1.** $^1$H NMR spectrum (400 MHz, 298 K, $CD_2Cl_2$) of **4**. *Residual solvent peaks.

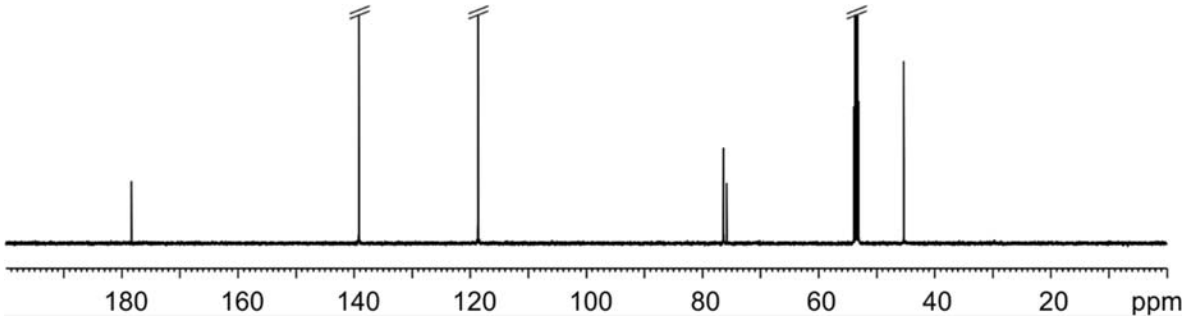


**Figure S 2.** $^{13}$C{$^1$H} NMR (100 MHz, 298 K, $CD_2Cl_2$) of **4**.

### 2.2.Synthesis of 1,4-disubstituted 1,2,3-triazole pyridyl *N*-oxide derivatives.

General procedure for the synthesis of ditopic 1,4-disubstituted 1,2,3-triazole pyridine-*N*-oxide derivatives **7a**, **7b**, and **7c**. Ditopic 1,4-disubstituted 1,2,3-triazole derivatives were obtained through a 1,3-dipolar cycloaddition reaction between para-substituted pyridine-*N*-oxide precursors with azide terminal groups and the 1-(2-propynyl)-4-pyridinone **4**. In general, the pyridine-*N*-oxide azide derivative (0.1 mmol) and 1-(2-propynyl)-4-pyridinone (0.1 mmol) were dissolved in 5 mL of dry dichloromethane under argon. Then, $Cu(CH_3CN)_4PF_6$ (5 µmol, 0.05 equiv.) and tris[(1-benzyl-1*H*-1,2,3-triazol-4-yl)methyl]amine (TBTA) (5 µmol, 0.05 equiv.) were added to the mixture and stirred for 2 h at r.t. protected from light. A white precipitate was formed in the reaction mixture. The white precipitate was collected via filtration and washed with dichloromethane (5 mL) and acetonitrile (5 mL) to provide pure products **7a-c** in 72-88 % yield.

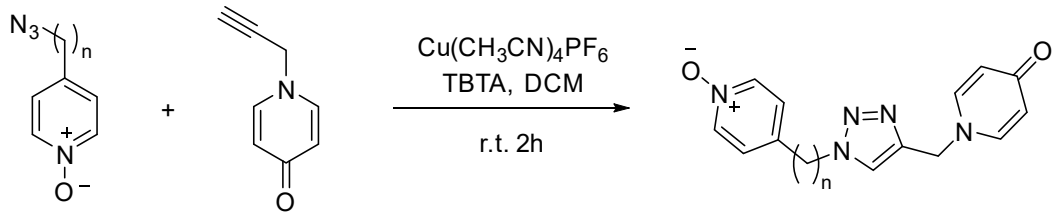


**Scheme S 1.** Synthesis of 1,4-disubstituted 1,2,3-triazole derivatives **7a** (n = 0), **7b** (n = 1), and **7c** (n = 2).

**7a**: 4-Azido pyridine-*N*-oxide **2a** and 1-(2-propynyl)-4-pyridinone **4** were used to prepare compound **7a** (88 % yield) using the general procedure described above.

$^1$H NMR (400 MHz, 298 K, $d_6$-DMSO): δ (ppm) = 8.93 (s, 1H), 8.40 (d, $J$ = 6.8 Hz, 2H), 8.00 (d, $J$ = 6.8 Hz, 2H), 7.81 (s, 2H), 6.11 (s, 2H), 5.27 (s, 2H). $^{13}$C{$^1$H} NMR (100 MHz, 298K, $d_6$-DMSO): δ (ppm) = 177.8, 144.5, 141.6, 140.7, 132.6, 122.7, 121.1 (br), 117.8, 50.1. HR-MS (ESI TOF) m/z: $[M+Na]^+$ calculated for $C_{13}H_{11}N_5NaO_2^+$ = 292.0805, found 292.0810.

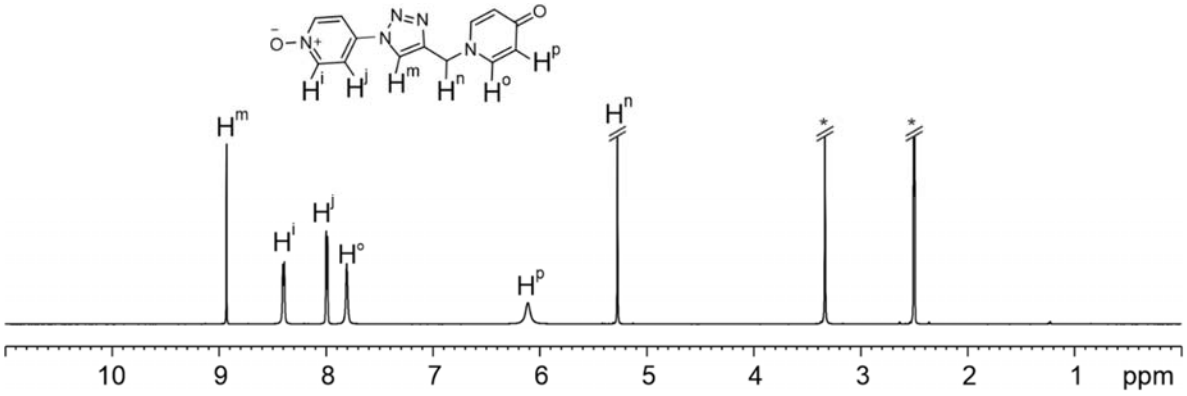


**Figure S 3.** $^1$H NMR spectrum (400 MHz, 298 K, $d_6$-DMSO) of **7a**. *Residual solvent peaks.

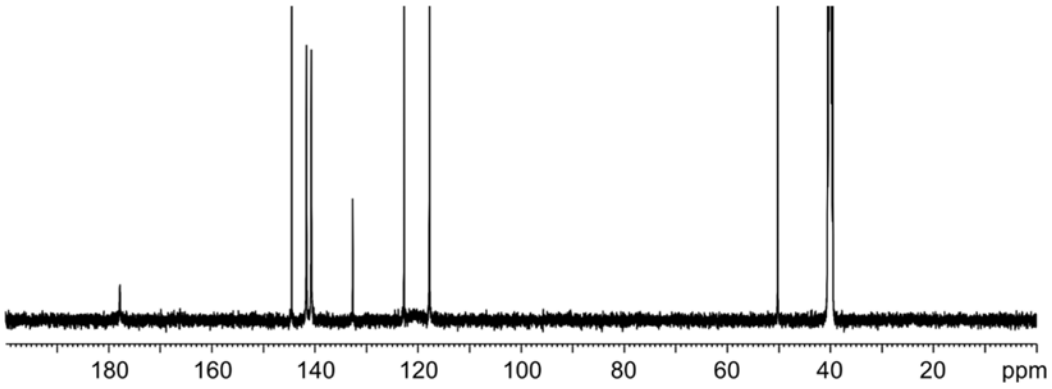


**Figure S 4.** $^{13}C\{^{1}H\}$ NMR (100 MHz, 298 K, $d_6$-DMSO) of **7a,**

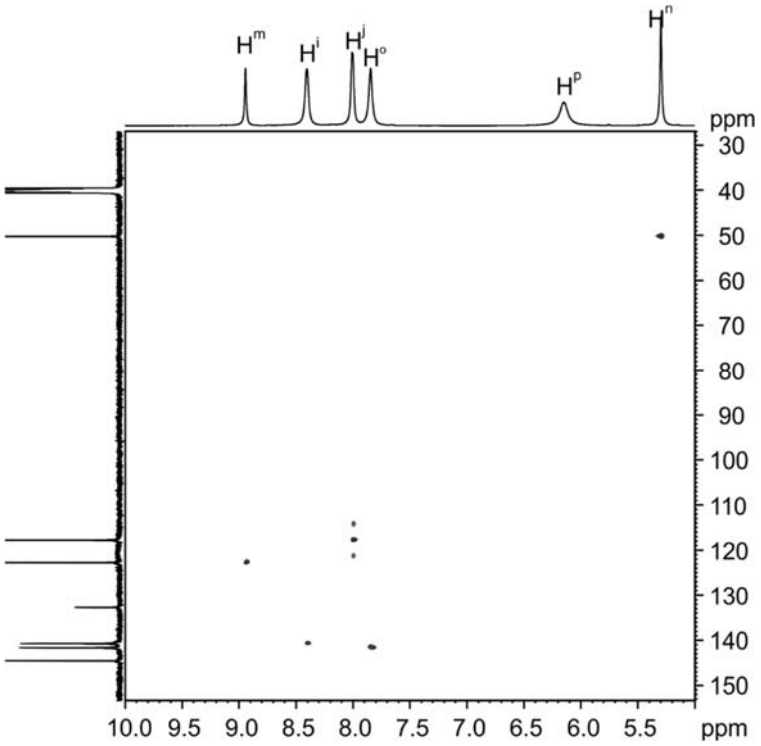


**Figure S 5.** Selected region of $^{1}H$-$^{13}C$ HSQC NMR (400 MHz, 298 K, $d_6$-DMSO) of **7a**.

**7b**: 4-azidomethyl pyridine-*N*-oxide **2b** and 1-(2-propynyl)-4-pyridinone **4** were used for the preparation of compound **7b** (81 % yield) using the general procedure described above.

$^{1}H$ NMR (400 MHz, 298 K, $d_6$-DMSO): δ (ppm) = 8.23 (s, 1H), 8.2 (d, $J$ = 6.8 Hz, 2H), 7.73 (d, $J$ = 6.4 Hz, 2H), 7.30 (d, $J$ = 6.8 Hz, 2H), 6.08 (d, $J$ = 6.4 Hz, 2H), 5.62 (s, 2H), 5.15 (s, 2H) ppm. $^{13}C\{^{1}H\}$ NMR (100 MHz, 298K, $d_6$-DMSO): δ (ppm) = 177.6, 143.4, 141.4, 139.4, 133.4, 126.4,

124.7, 118.6 (br), 51.2, 50.2. HR-MS (ESI TOF) m/z: $[M+H]^+$ calculated for $C_{14}H_{14}N_5O_2^+$ = 284.1142, found 284.1126.

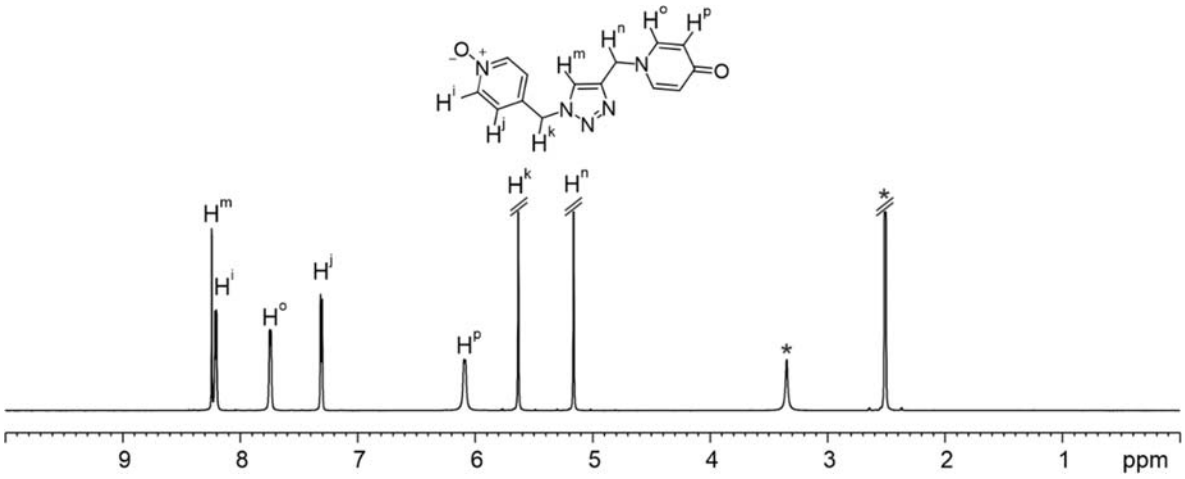


**Figure S 6.** $^1$H NMR spectrum (400 MHz, 298 K, $d_6$-DMSO) of **7b**. *Residual solvent peaks.

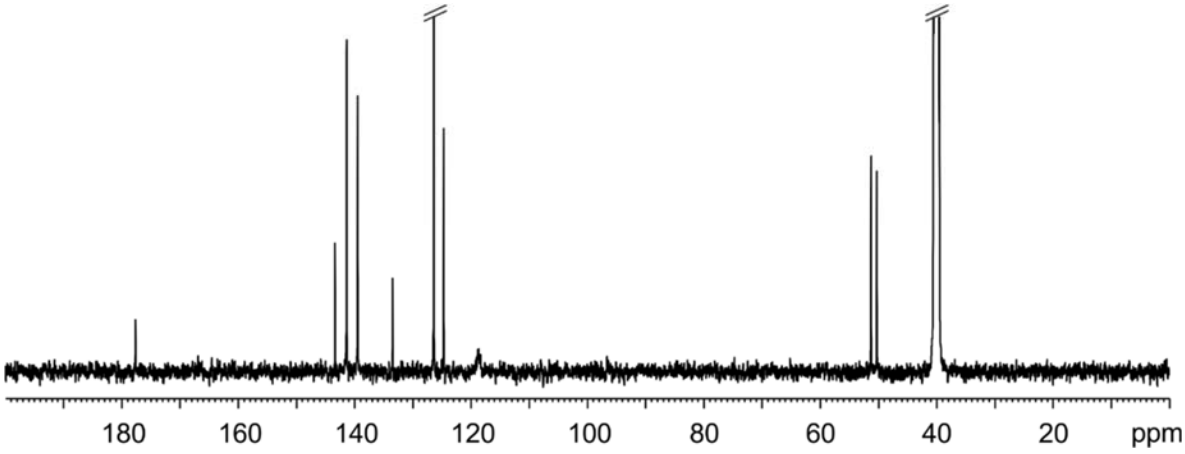


**Figure S 7.** $^{13}C\{^1H\}$ NMR (100 MHz, 298 K, $d_6$-DMSO) of **7b**.

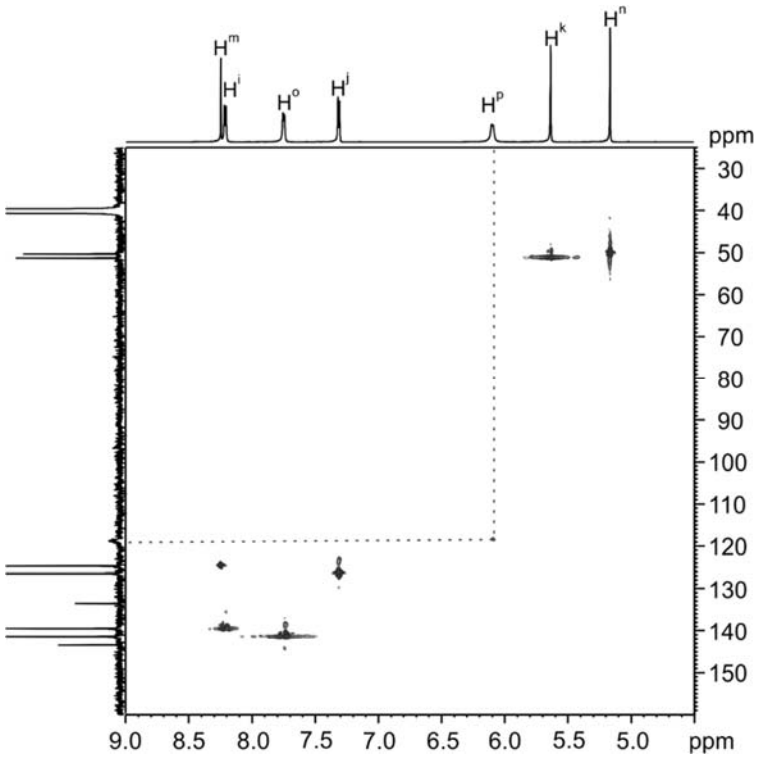


**Figure S 8.** Selected region of $^{1}$H-$^{13}$C HSQC NMR (400 MHz, 298 K, *d*$_6$-DMSO) of **7b**.

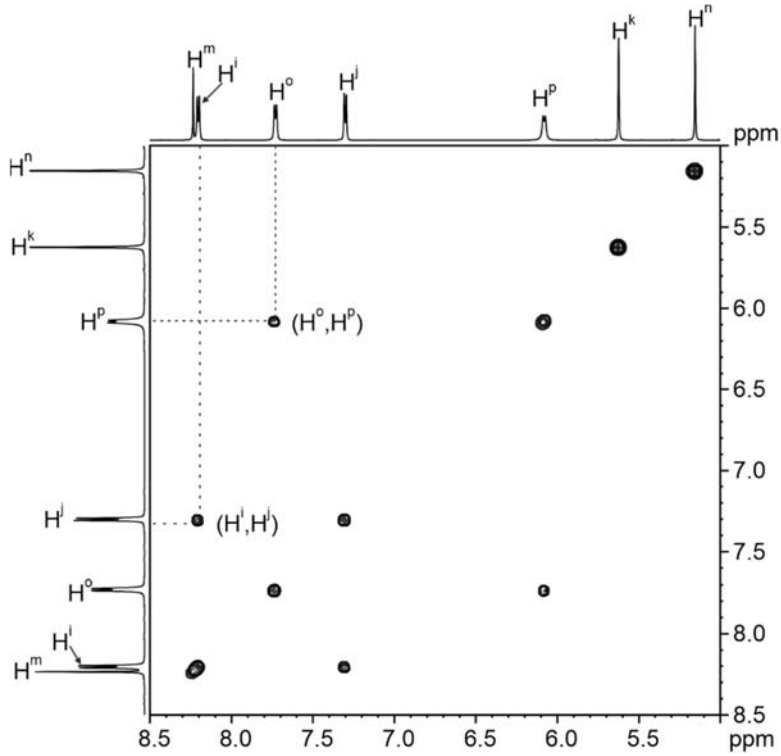


**Figure S 9.** Selected region of $^{1}$H-$^{1}$H COSY NMR (400 MHz, 298 K, $d_6$-DMSO) of **7b**.

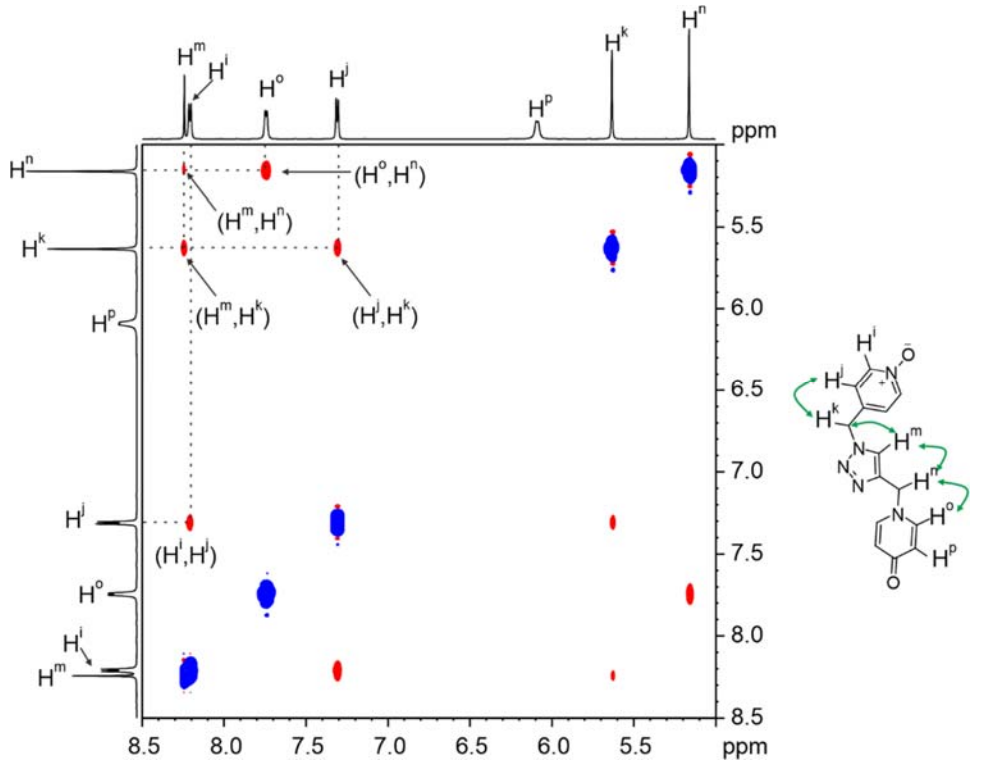


**Figure S 10.** Selected region of $^{1}$H-$^{1}$H NOESY NMR (400 MHz, 298 K, *d*$_6$-DMSO, D8 = 0.6 s) of **7b**.

**7c**: 4-azidoethyl pyridine-*N*-oxide **2c** and 1-(2-propynyl)-4-pyridinone **4** were used for the preparation of compound **7c** (72 % yield) using the general procedure described above.

$^{1}$H NMR (400 MHz, 298 K, *d*$_6$-DMSO): δ (ppm) = 8.07 (d, *J* = 6.8 Hz, 2H), 8.05 (s, 1H), 7.66 (d, *J* = 7.6 Hz, 2H), 7.18 (d, *J* = 6.8 Hz, 2H), 6.08 (d, *J* = 7.6 Hz, 2H), 5.11 (s, 2H), 4.64 (t, *J* = 7.0 Hz, 2H), 3.14 (t, *J* = 7.0 Hz, 2H) ppm. $^{13}$C{$^{1}$H} NMR (100 MHz, 298K, *d*$_6$-DMSO): δ (ppm) = 177.6, 142.8, 141.1, 138.8, 136.0, 127.2, 124.4, 118.0, 50.2, 49.9, 34.4. HR-MS (ESI TOF) m/z: $[M+H]^+$ calculated for $C_{15}H_{16}N_5O_2^+$ = 298.1299, found 298.1293.

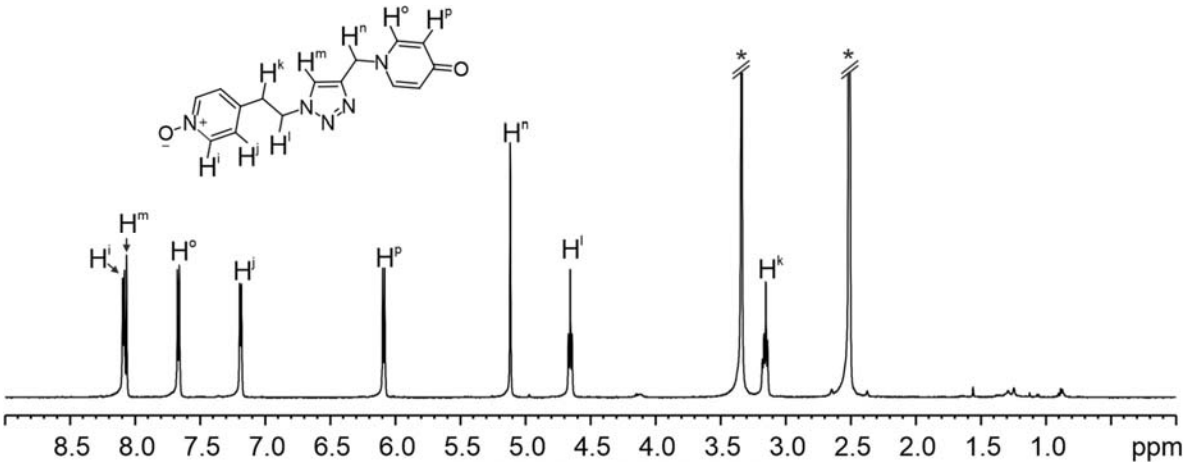


**Figure S 11.** $^{1}$H NMR spectrum (400 MHz, 298 K, $d_6$-DMSO) of **7c**. *Residual solvent peaks.

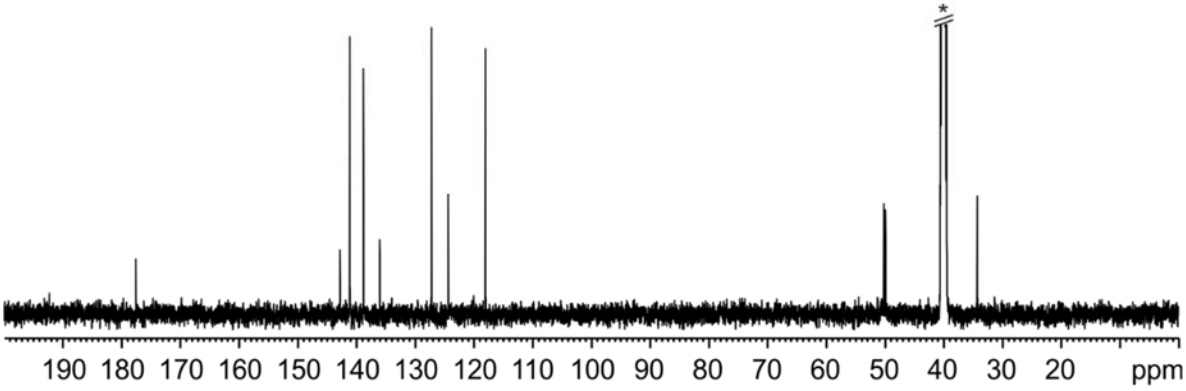


**Figure S 12.** $^{13}$C{$^{1}$H} NMR (100 MHz, 298 K, $d_6$-DMSO) of **7c**.

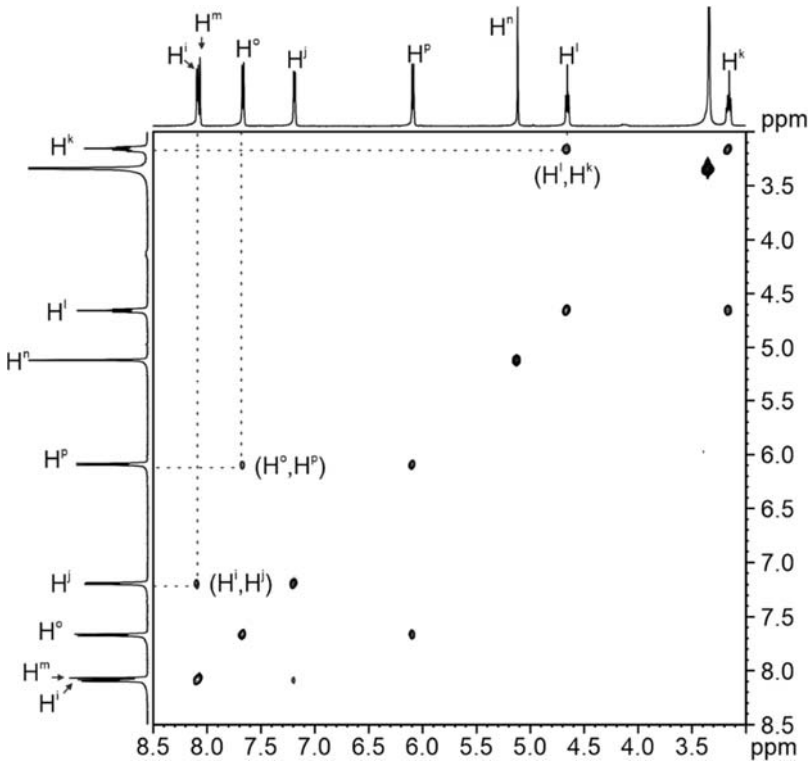


**Figure S 13.** Selected region of $^{1}$H-$^{1}$H COSY NMR (400 MHz, 298 K, $d_6$-DMSO) of **7c**.

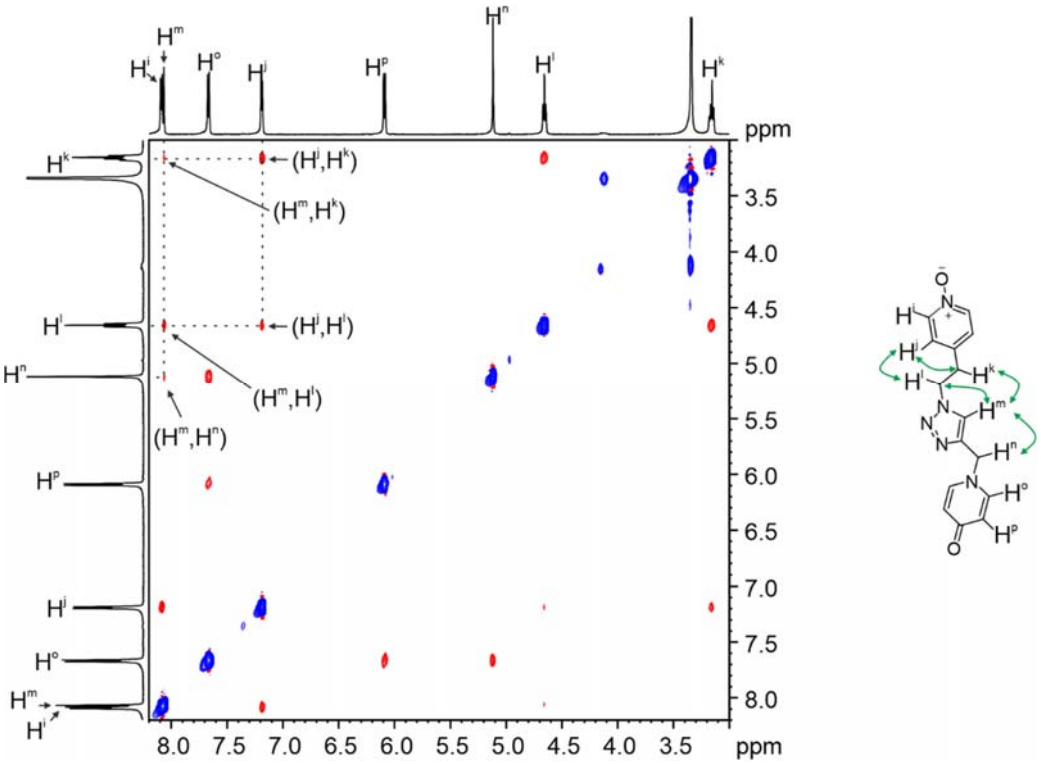


**Figure S 14.** Selected region of $^{1}$H-$^{1}$H NOESY NMR (400 MHz, 298 K, $d_6$-DMSO, D8 = 0.6 s) of **7c**.

### 2.3. Synthesis of 1,5-disubstituted 1,2,3-triazole pyridine-*N*-oxide derivatives.

General procedure for synthesizing ditopic 1,5-disubstituted 1,2,3-triazole pyridine-*N*-oxide derivatives **8b** and **8c**. Analytical quantities of 1,5-disubstituted 1,2,3-triazole derivatives were synthesized via uncatalyzed thermal 1,3-dipolar cycloaddition reaction between the para-substituted azido(alkyl) pyridine-*N*-oxides **2b-c** and 1-(2-propynyl)-4-pyridinone **4**. In general, the azido(alkyl) pyridine-*N*-oxides (1.0 mmol) and 1-(2-propynyl)-4-pyridinone **4** (1.0 mmol) were dissolved in 10 mL of dry DMF under argon atmosphere. The mixture was stirred for 24 h at 70 $^{o}$C protected from light. After that, the solvent was evaporated under vacuum to give the reaction crude mixture containing the two isomeric products (1,4- and 1,5-triazole derivatives) and the starting materials. The 1,5-disubstituted 1,2,3-triazole pyridine-*N*-oxide **8b** and **8c** were obtained after HPLC purification of the reaction crudes using an analytical BEH HILIC column (3.5 µm, 4.6×150 mm, Waters Xbridge®) with the corresponding precolumn (3.5 µm, 3.9 mm × 5mm, Waters Xbridge®) and a linear solvent gradient elution $CH_3CN$:$H_2O$ (98:2 to 60:40 in 15 minutes). We used 276 nm as detection wavelength.

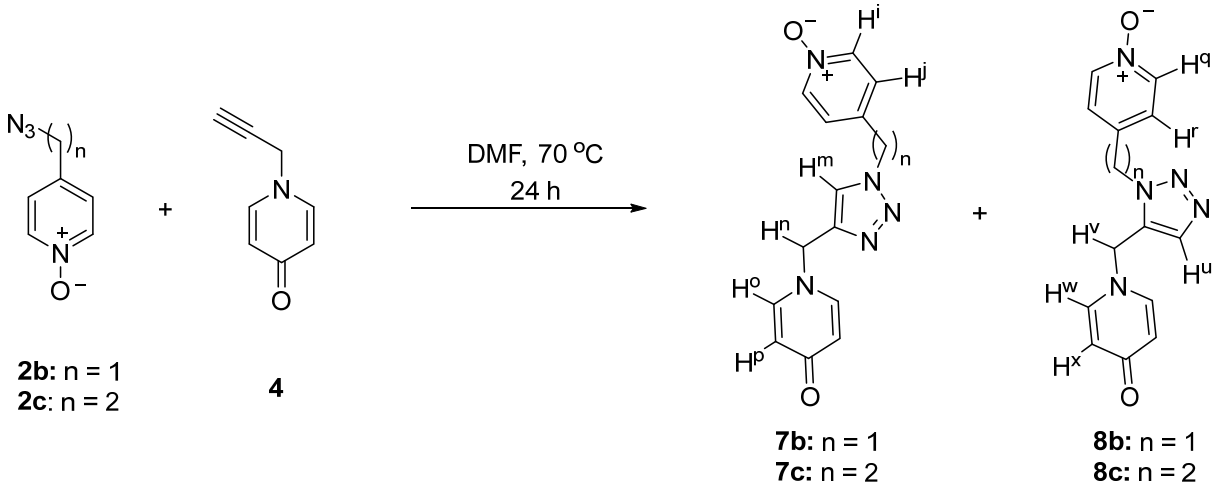


**Scheme S 2.** Synthesis of ditopic pyridine-*N*-oxide 1,4-disubstituted 1,2,3-triazole derivatives **7b**, **7c** and 1,5-disubstituted 1,2,3-triazole derivatives **8b**, **8c**.

**8b**: 4-azido(methyl) pyridine-*N*-oxide **2b** and 1-(2-propynyl)-4-pyridinone **4** were used to prepare compound **8b** using the general procedure described above. Analytical amounts of compound **8b** (1 mg) were obtained after HPLC purification of the reaction crude using an analytical BEH HILIC column (3.5 µm, 4.6×150 mm, Waters Xbridge®) and a linear solvent gradient elution $CH_3CN$:$H_2O$ (98:2 to 60:40 in 15 minutes). We combined the fractions eluting at 12.7 min of 40 consecutive injections of 10 µL of the reaction crude (10 mg/mL in MeOH) and evaporated the solvent to afford **8b** as a white solid (~1 mg).

$^1$H NMR (400 MHz, 298 K, $d_6$-DMSO): δ (ppm) = 8.14 (d, $J$ = 7.2 Hz, 2H), 7.79 (s, 1H), 7.62 (d, $J$ = 7.8 Hz, 2H), 7.06 (d, $J$ = 7.2 Hz, 2H), 6.01 (d, $J$ = 7.8 Hz, 2H), 5.71 (s, 2H), 5.28 (s, 2H) ppm. $^{13}$C{$^1$H} NMR (100 MHz, 298K, $d_6$-DMSO): δ (ppm) = 177.0, 140.6, 138.8, 134.0, 133.7, 132.7, 125.0, 117.7, 48.8, 46.7. HR-MS (ESI TOF) m/z: $[M+Na]^+$ calculated for $C_{14}H_{13}N_5NaO_2^+$ = 306.0961, found 306.0974.

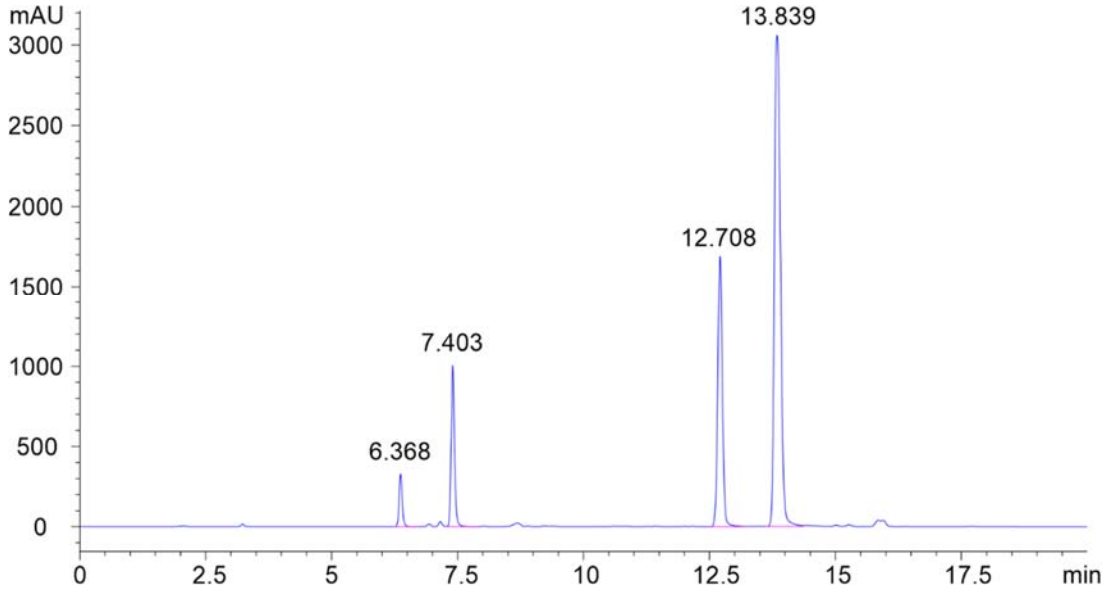


**Figure S 15.** Chromatogram of the reaction crude of **2b** and **4** (10 mg/mL solution) using 276 nm detection wavelength.

**Table S 1.** Retention times of compounds **2b**, **4**, **8b,** and **7b** in the reaction crude using an analytical BEH HILIC column (3.5 µm, 4.6×150 mm, Waters Xbridge®, 1 mL/min) and a linear solvent gradient elution $CH_3CN$:$H_2O$ (98:2 to 60:40 in 15 minutes).

| Peak | Retention time (min) | Compound |
|---|---|---|
| 1 | 6.4 | **2b** |
| 2 | 7.4 | **4** |
| 3 | 12.7 | **8b** |
| 4 | 13.8 | **7b** |

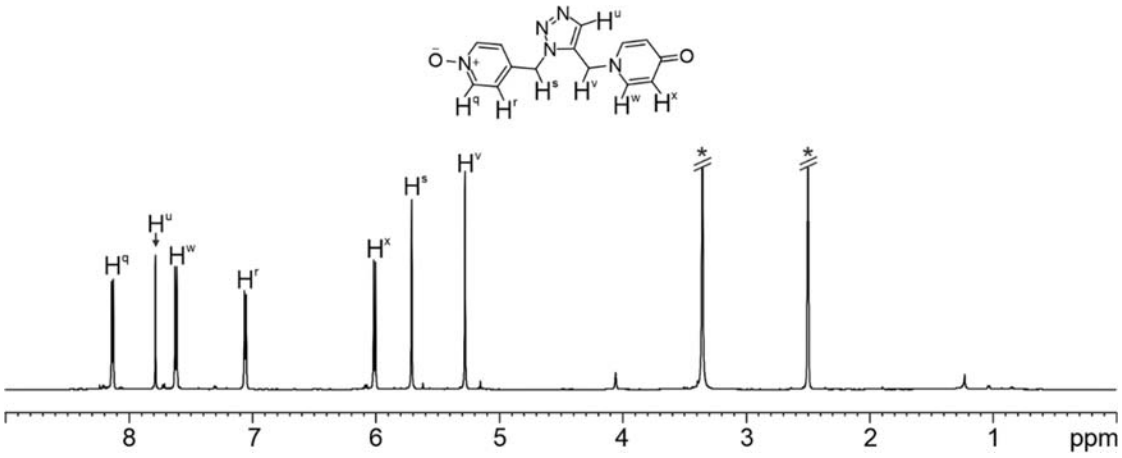


**Figure S 16.** $^{1}$H NMR spectrum (400 MHz, 298 K, $d_6$-DMSO) of **8b**. *Residual solvent peaks.

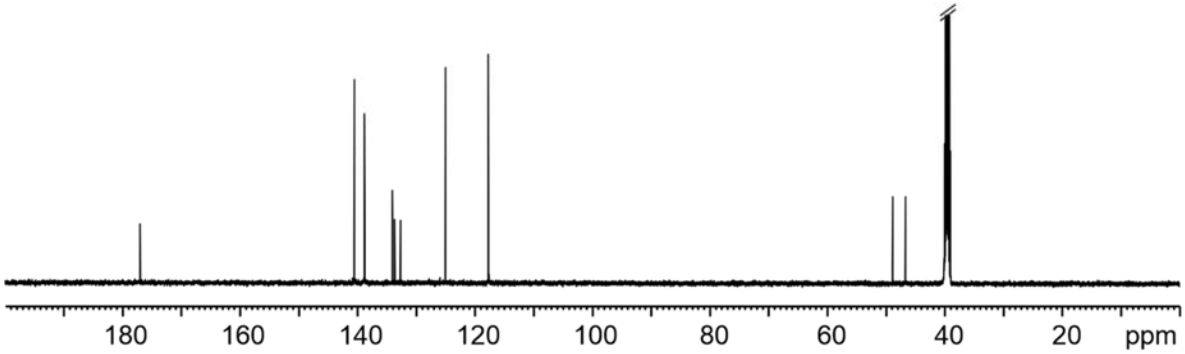


**Figure S 17.** $^{13}$C{$^{1}$H} NMR (100 MHz, 298 K, $d_6$-DMSO) of **8b**.

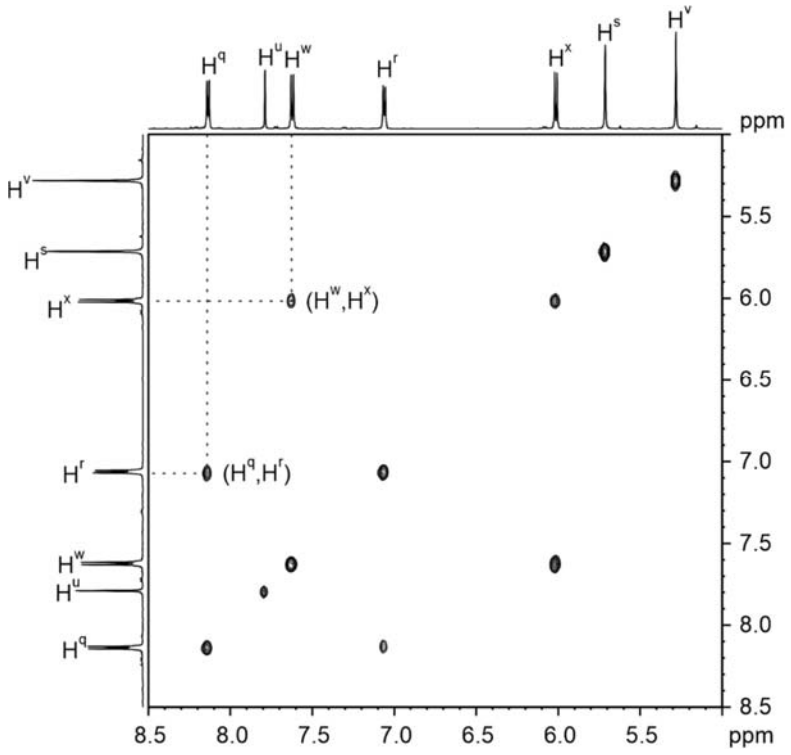


**Figure S 18.** Selected region of $^{1}$H-$^{1}$H COSY NMR (400 MHz, 298 K, $d_6$-DMSO) of **8b**.

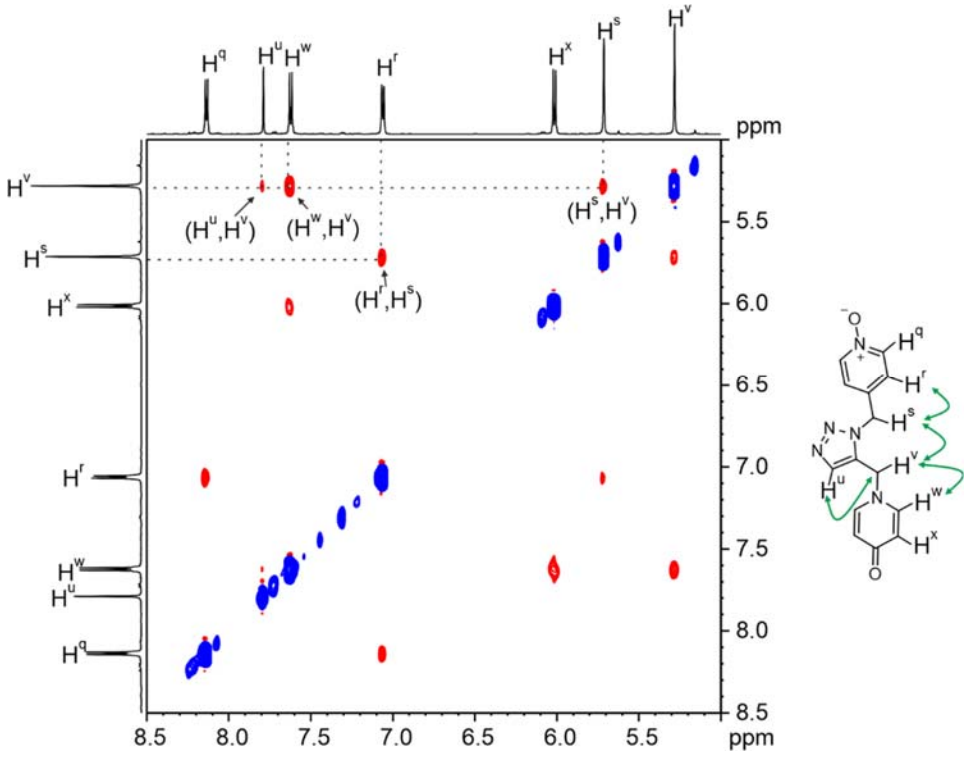


**Figure S 19.** Selected region of $^{1}$H-$^{1}$H NOESY NMR (400 MHz, 298 K, $d_6$-DMSO, D8 = 0.6 s) of **8b**.

**8c**: 4-azido(ethyl) pyridine-*N*-oxide **2c** and 1-(2-propynyl)-4-pyridinone **4** were used to prepare compound **8c** using the general procedure described above. Analytical amounts of compound **8c** (1 mg) were obtained after HPLC purification of the reaction crude using an analytical BEH HILIC column (3.5 µm, 4.6×150 mm, Waters Xbridge®, 1 mL/min) and a linear solvent gradient elution $CH_3CN$:$H_2O$ (98:2 to 60:40 in 15 minutes). We combined the fractions eluting at 13.9 min of 40 consecutive injections of 10 µL of the reaction crude (10 mg/mL in MeOH) and evaporated the solvent to afford **8c** as a white solid (~1 mg).

$^1$H NMR (400 MHz, 298 K, $d_6$-DMSO): δ (ppm) = 8.12 (d, *J* = 7.0 Hz, 2H), 7.71 (d, *J* = 7.6 Hz, 2H), 7.65 (s, 1H), 7.21 (d, *J* = 7.0 Hz, 2H), 6.13 (d, *J* = 7.6 Hz, 2H), 5.30 (s, 2H), 4.64 (t, *J* = 7.3 Hz, 2H), 3.06 (t, *J* = 7.3 Hz, 2H) ppm. $^{13}$C{$^1$H} NMR (100 MHz, 298K, $d_6$-DMSO): δ (ppm) = 177.6, 141.1, 138.8, 135.7, 133.9, 133.7, 127.4, 118.4, 47.9, 47.3, 33.9. HR-MS (ESI TOF) m/z: $[M+H]^+$ calculated for $C_{15}H_{16}N_5O_2^+$ = 298.1299, found 298.1293.

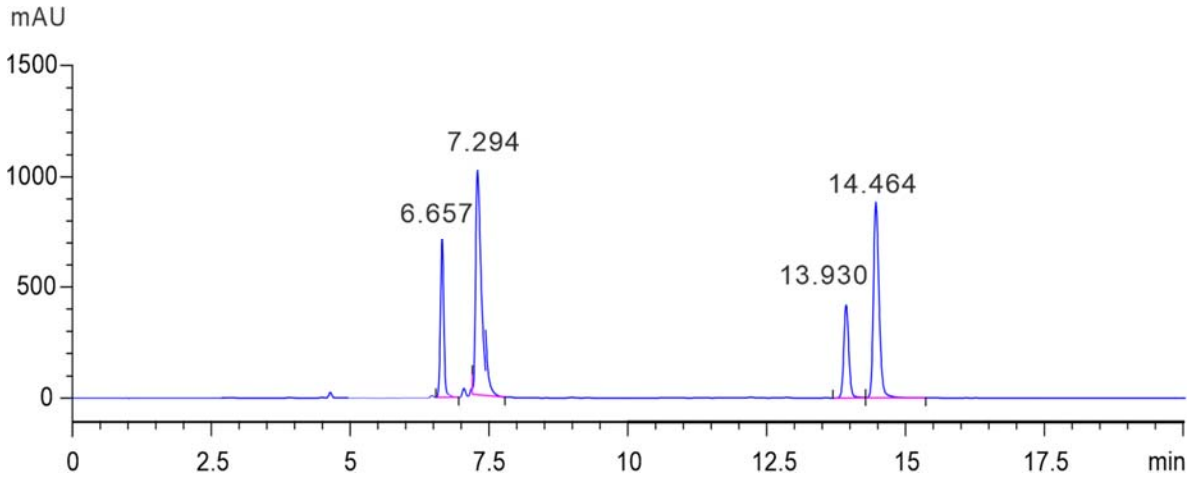


**Figure S 20.** Chromatogram of the reaction crude of **2c** and **4** (10 mg/mL solution) using 276 nm detection wavelength.

**Table S 2.** Retention times of compounds **2c**, **4**, **8c,** and **7c** in the reaction crude using an analytical BEH HILIC column (3.5 µm, 4.6×150 mm, Waters Xbridge®, 1 mL/min) and a linear solvent gradient elution $CH_3CN$:$H_2O$ (98:2 to 60:40 in 15 minutes).

| Peak | Retention time (min) | compound |
|---|---|---|
| 1 | 6.7 | **2c** |
| 2 | 7.3 | **4** |
| 3 | 13.9 | **8c** |
| 4 | 14.5 | **7c** |

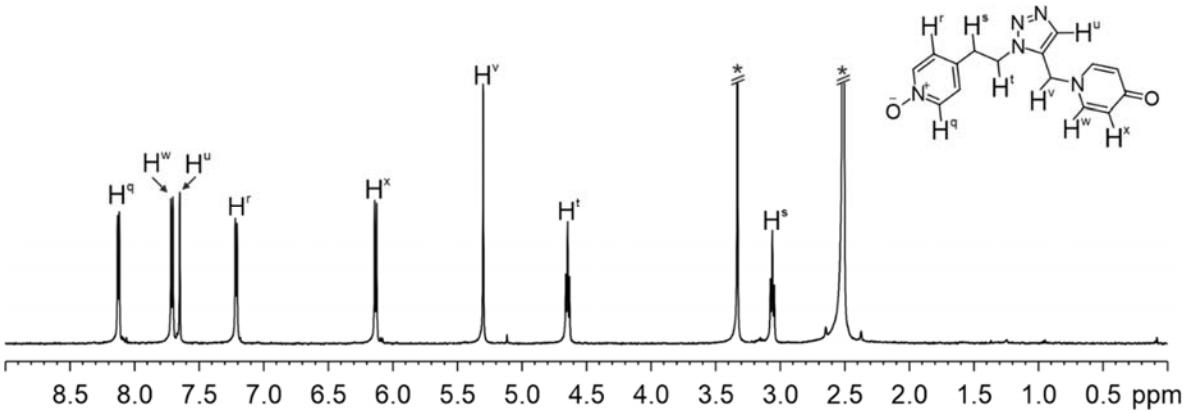


**Figure S 21.** $^{1}$H NMR spectrum (400 MHz, 298 K, $d_6$-DMSO) of **8c**. *Residual solvent peaks.

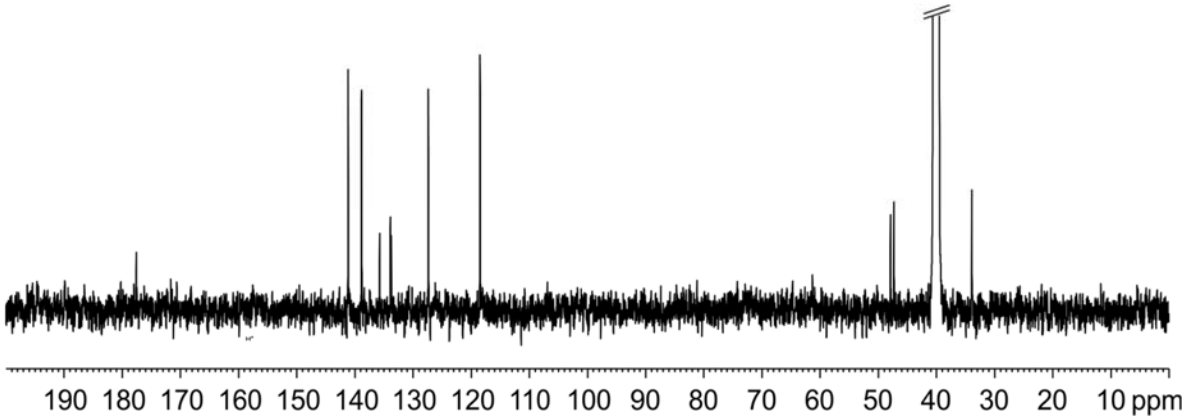


**Figure S 22.** $^{13}$C{$^{1}$H} NMR (100 MHz, 298 K, $d_6$-DMSO) of **8c**.

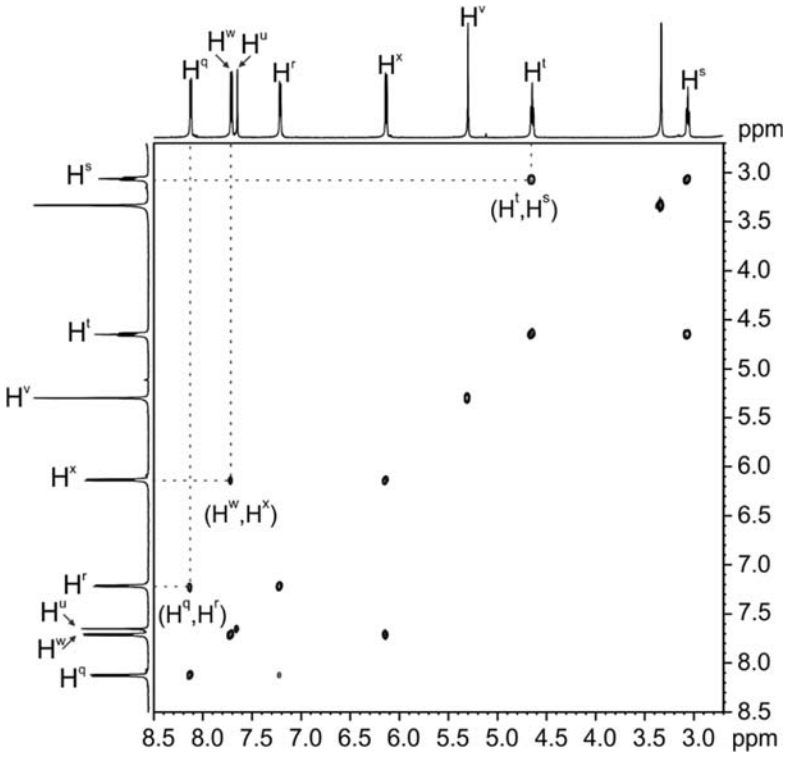


**Figure S 23.** Selected region of $^{1}$H-$^{1}$H COSY NMR (400 MHz, 298 K, $d_6$-DMSO) of **8c**.

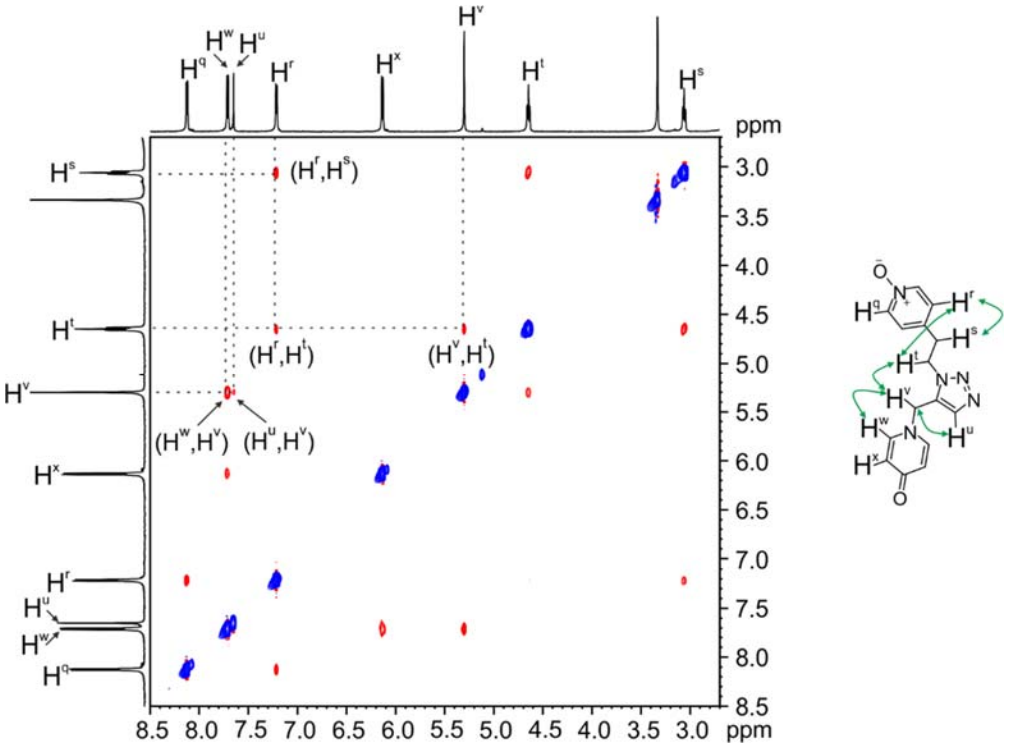


**Figure S 24.** Selected region of $^{1}$H-$^{1}$H NOESY NMR (400 MHz, 298 K, $d_6$-DMSO, D8 = 0.6 s) of **8c**.

## 3. Binding studies and characterization of octa-imine cage 1 with monotopic 1-(2-propynyl)-4-pyridinone 4 and disubstituted 1,2,3-triazole derivatives 7 and 8 in $CDCl_3$: $CD_3CN$ 9:1 mixture.

### 3.1. Binding studies of 1-(2-propynyl)-4-pyridinone 4 with 1.

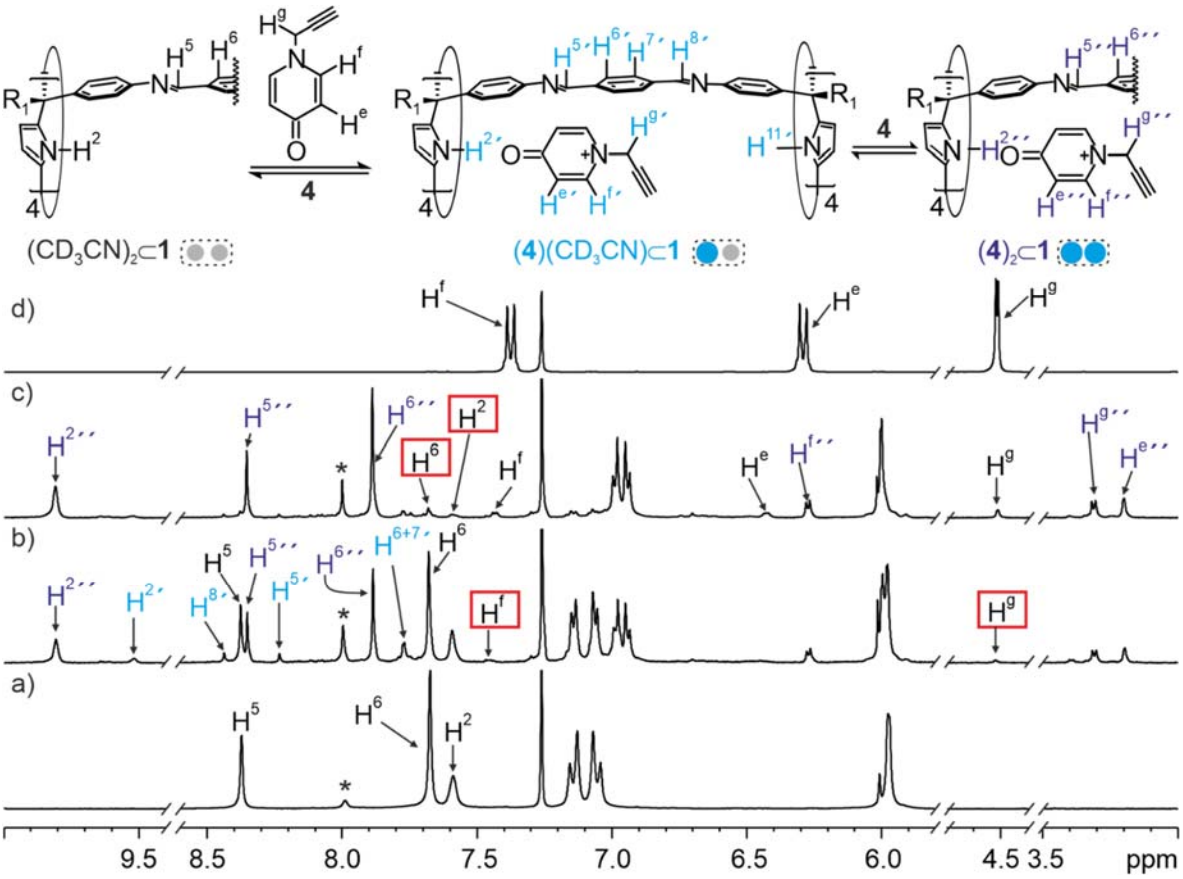


**Figure S 25.** Selected regions of the $^1$H NMR (400 MHz, 298 K, $CDCl_3$:$CD_3CN$ 9:1) spectra of the titration of a 2 mM solution of octa-imine cage **1**, upon addition of a) 0 equiv., b) 1 equiv., c) 2 equiv. of **4**. Spectrum d) corresponds to the free **4** in the same solvent mixture. Primed and double-primed proton signals correspond to those of the 1:1 and 2:1 complexes, respectively. *Residual peak related to the excess of terephthaldehyde linker in the cage synthesis process.

### 3.2. Co-inclusion of 4-azido pyridine-*N*-oxide 2a and 1-(2-propynyl)-4-pyridinone 4 in 1.

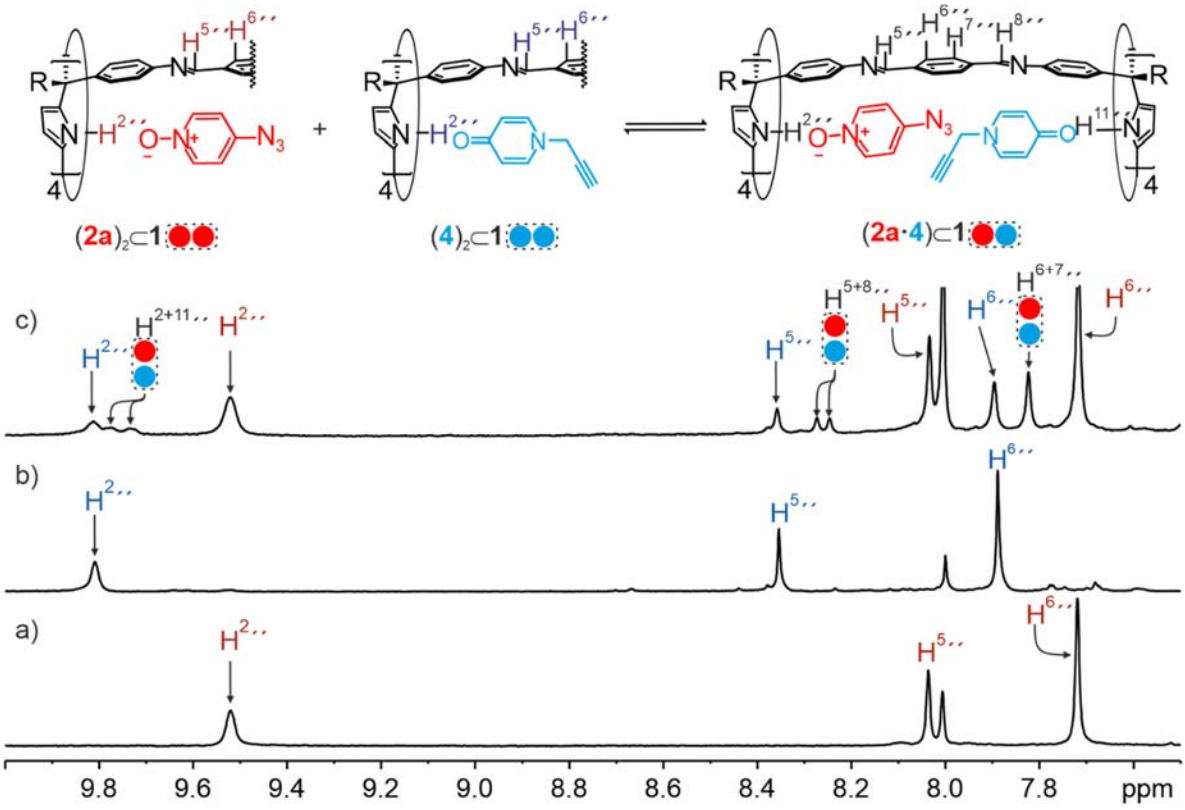


**Figure S 26.** Selected regions of $^{1}$H NMR (400 MHz, 298K, $CDCl_3$:$CD_3CN$ 9:1) spectra of solutions containing: a) 1:2 mixture of cage **1** and **2a**; b) 1:2 mixture of cage **1** and **4**; and c) 1:1:1 mixture of **1**:**2a**:**4**. Double primed protons correspond to the homo- and hetero- 2:1 complexes. Proton assignments in blue correspond to complexes with **4,** and proton assignments in red to complexes with **2a**.

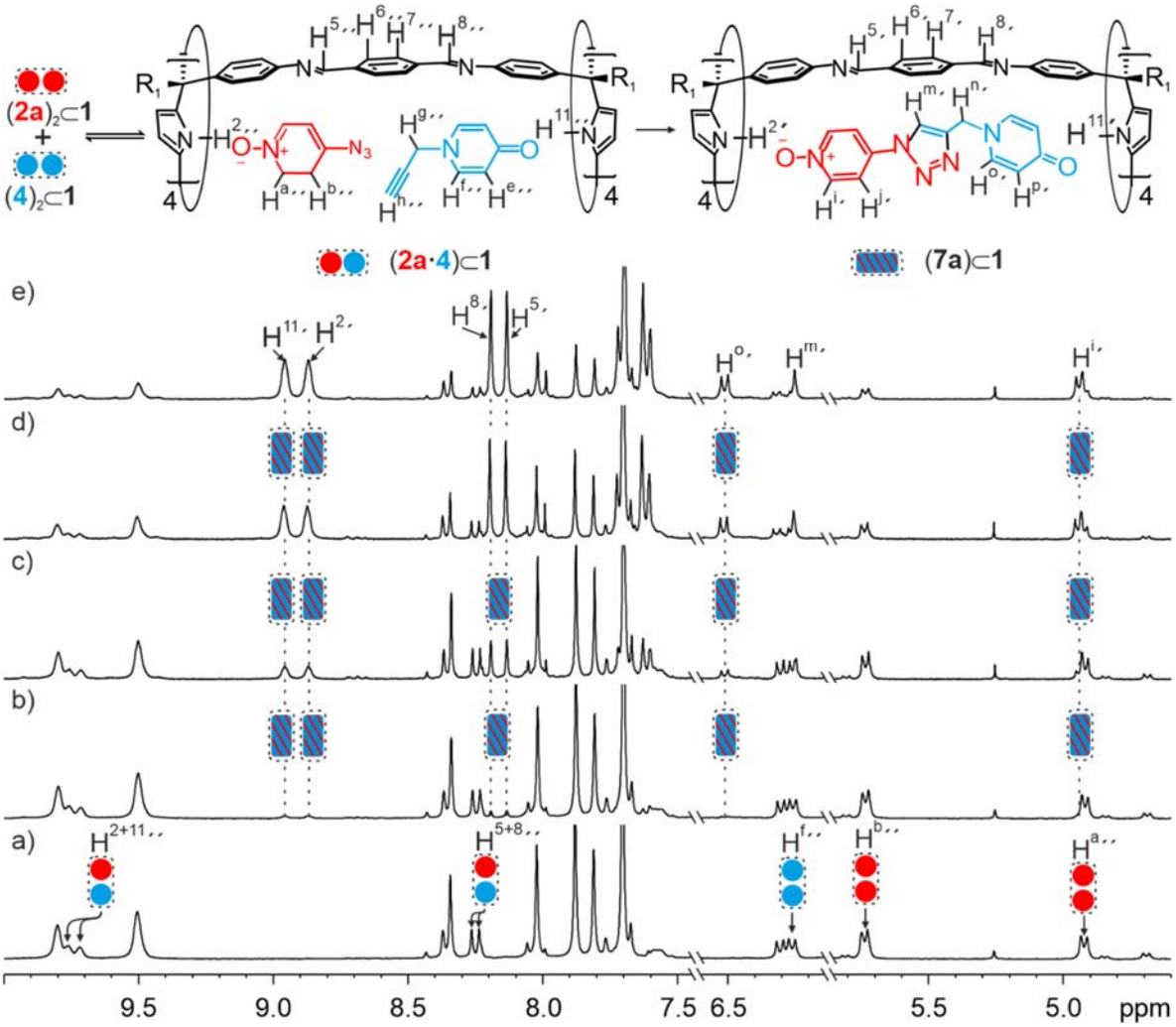


**Figure S 27.** Top) The 1,3-dipolar cycloaddition reaction between **2a** and **4** included in the octa-imine cage **1** yielded the complex **7a⊂1**. (Bottom) Selected regions of the $^{1}$H NMR (300 MHz, 298 K, $CDCl_3$:$CD_3CN$ 9:1) spectra corresponding to the monitoring of the formation of complex **7a⊂1** starting from a 1:1:1 molar mixture of compounds **1**, **2a**, and **4**, respectively, after a) 0 h, b) 6 h, c) 72 h, d) 12 days, and e) 16 days. Primed and double-primed letters indicate the proton signals in the 1:1 complexes, and 2:1 homo- and hetero-complexes, respectively.

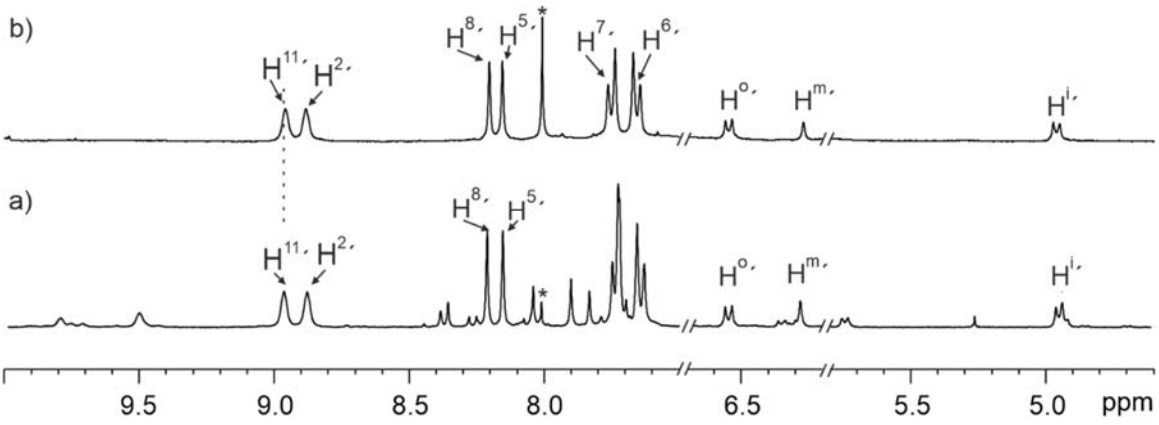


**Figure S 28.** a) Selected regions of the $^{1}$H NMR (300 MHz, 298 K, $CDCl_3$:$CD_3CN$ 9:1) spectra corresponding to the monitoring of the formation of complex **7a⊂1** starting from a 1:1:1 molar mixture of compounds **1**, **2a**, and **4** after 16 days. b) Spectrum of **7a⊂1** complex in the same solvent mixture. *Residual peak related to the excess of terephthaldehyde linker in the cage synthesis process.

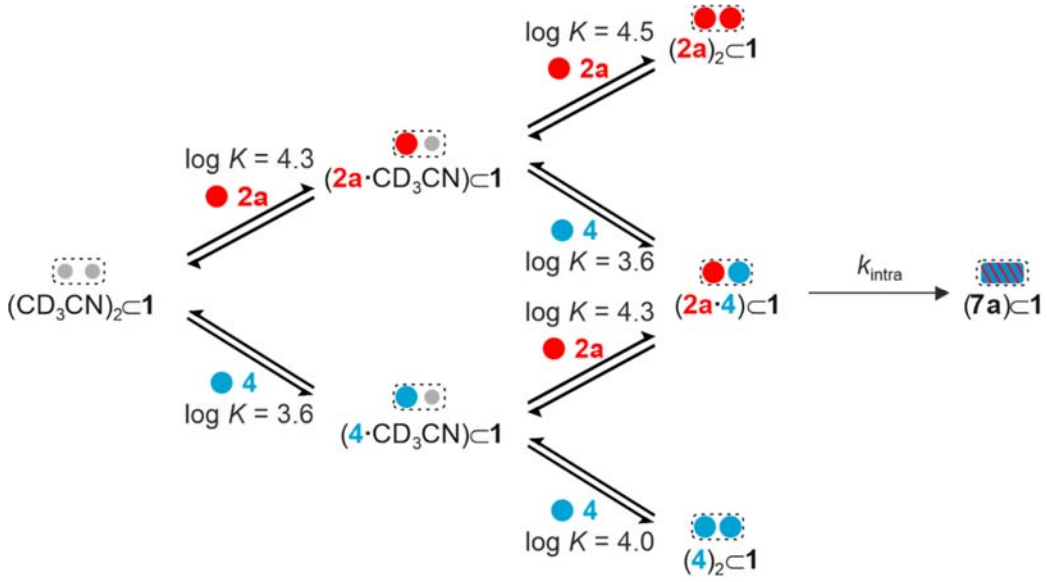


**Figure S 29.** Theoretical kinetic model used for the non-linear analysis of the experimental data, including the values for the thermodynamic equilibrium constants determined/estimated for each binding process. Red spheres correspond to 4-azido pyridine-*N*-oxide **2a**, blue spheres correspond to 1-(2-propynyl)-4-pyridinone **4,** and red-blue dashed cylinder corresponds to the cycloaddition product **7a**.

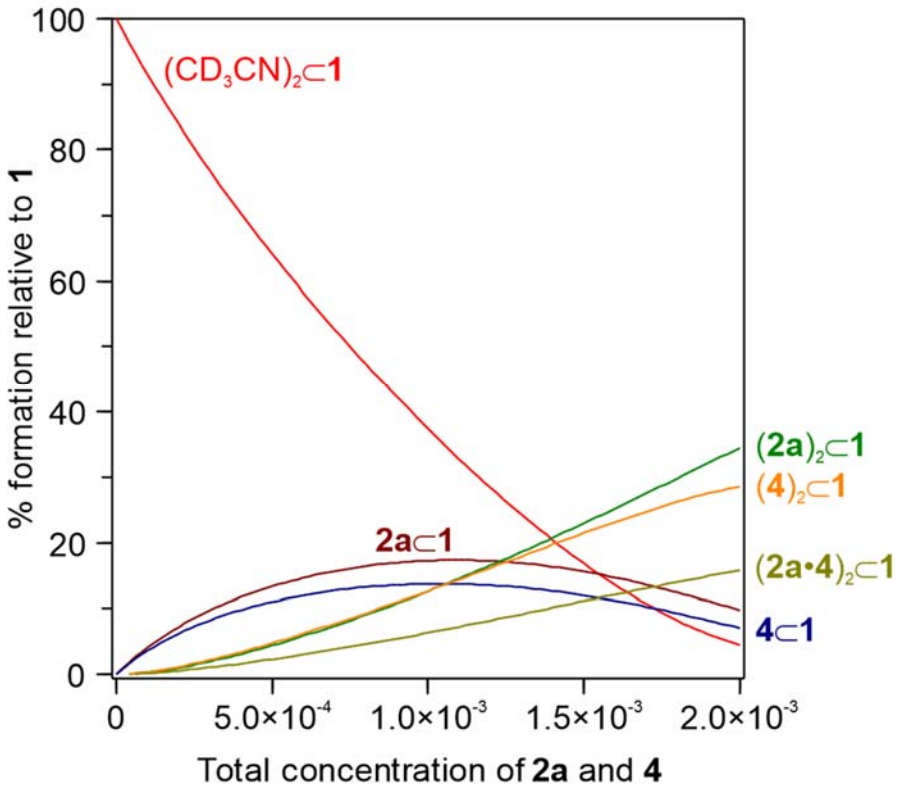


**Figure S 30.** Simulated speciation profile for octa-imine cage **1** (2 mM) with incremental amounts of **2a** (up to 2 mM) and **4** (up to 2 mM) determined using Hyperquad Simulation and Speciation (HySS2009) software using a model that considers the reversible formation of 1:1 and 2:1 homo- and hetero-inclusion complexes with the constants depicted in **Figure S 29**.

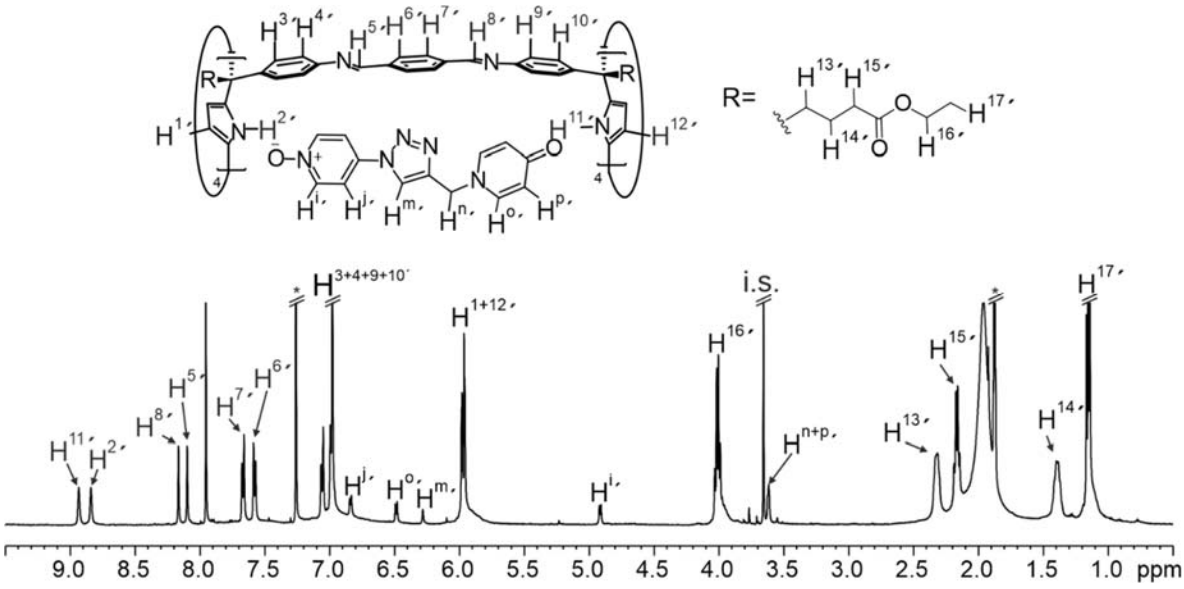


**Figure S 31.** $^{1}$H NMR spectrum (500 MHz, 298 K, $CDCl_3$:$CD_3CN$ 9:1) of **7a**⊂1 complex obtained from filtrated solution of solid-liquid extraction experiment of the insoluble guest **7a** with a mM solution of $(CD_3CN)_2$⊂1 in $CDCl_3$:$CD_3CN$ 9:1.

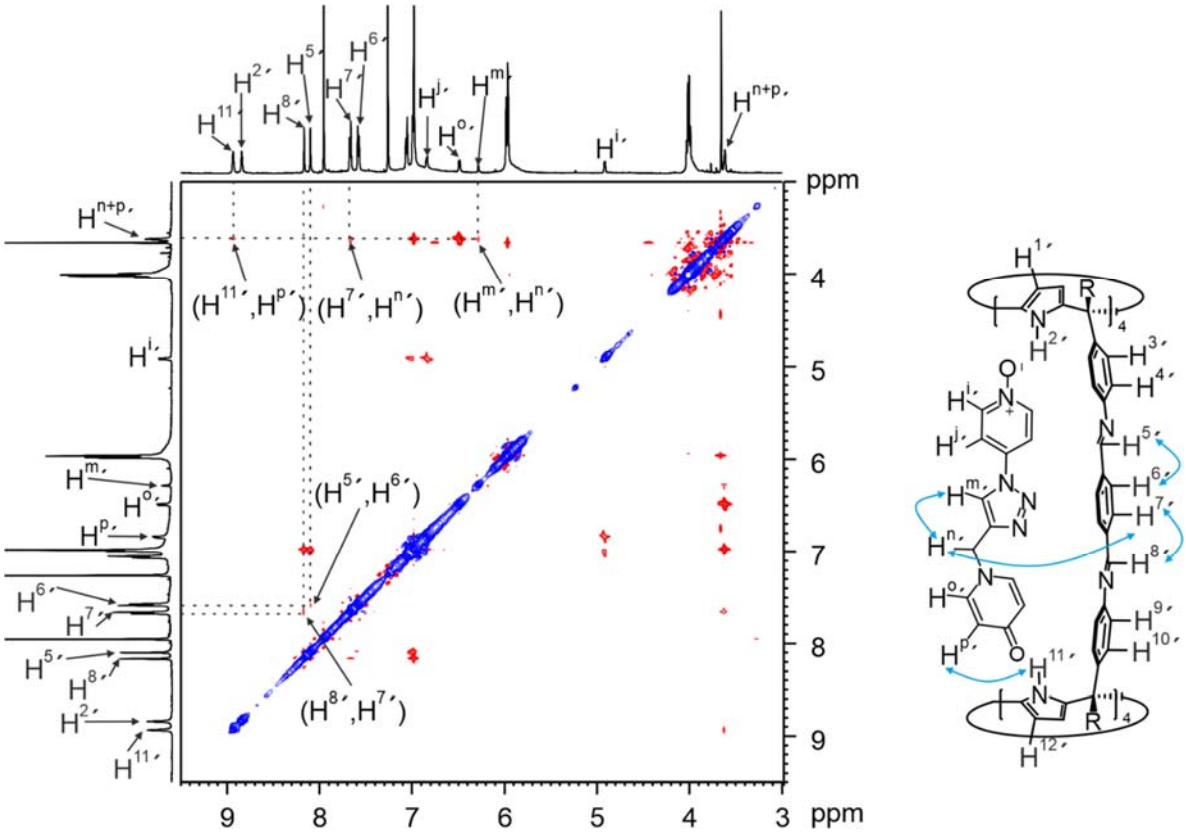


**Figure S 32.** Selected region of the $^{1}$H-$^{1}$H ROESY NMR (500 MHz, at 298 K, $CDCl_3$: $CD_3CN$ 9:1, D8 = 0.30 s) of **7a**⊂**1** complex.

### 3.3. Co-inclusion of 4-azido(methyl) pyridine-*N*-oxide 2b and 1-(2-propynyl)-4-pyridinone 4 in 1.

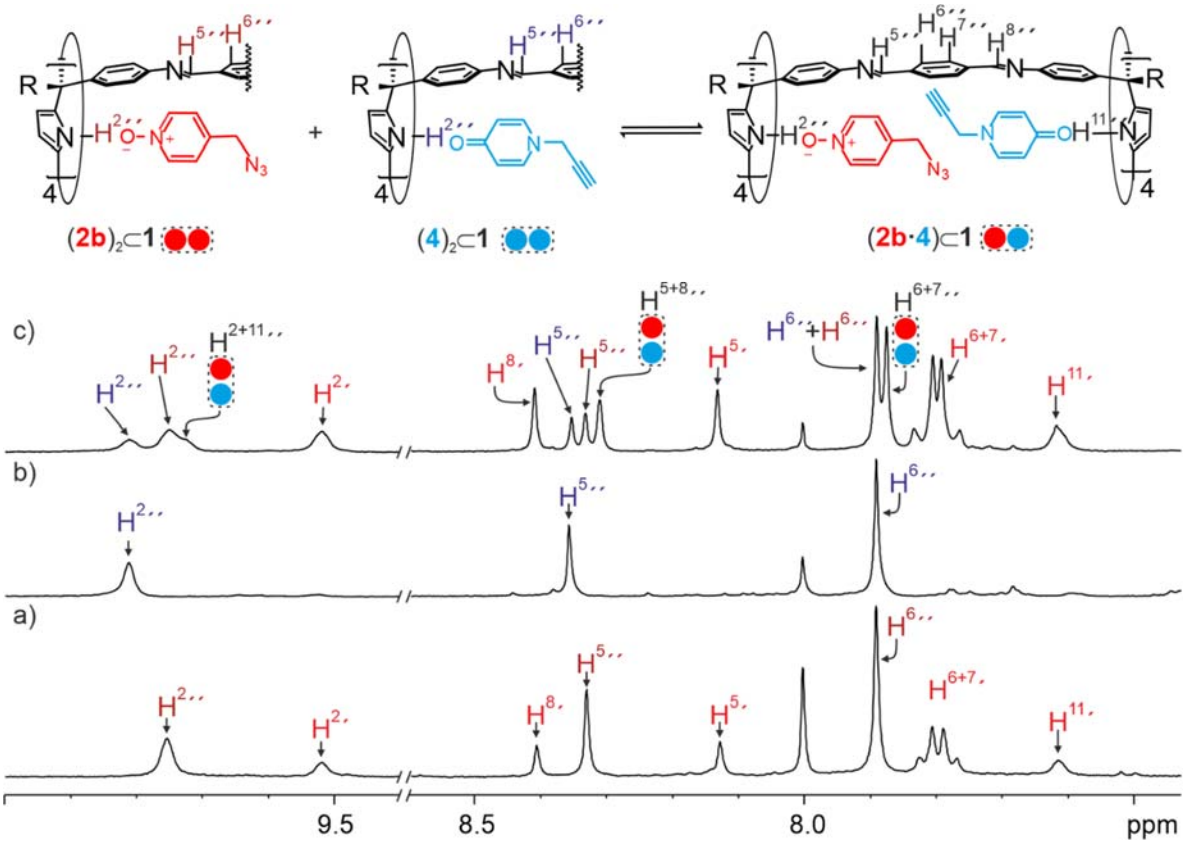


**Figure S 33.** Selected regions of $^{1}$H NMR (400 MHz, 298K, $CDCl_3$:$CD_3CN$ 9:1) spectra of solutions containing: a) 1:1.7 mixture of cage **1** and **2b**; b) 1:2 mixture of cage **1** and **4**; and c) 1:1:1 mixture of **1**:**2b**:**4**. Primed and double-primed protons correspond to the 1:1 and 2:1 complexes, respectively. Proton assignments in red correspond to the complexes with **2b** included, and those in blue correspond to the complexes with **4** included.

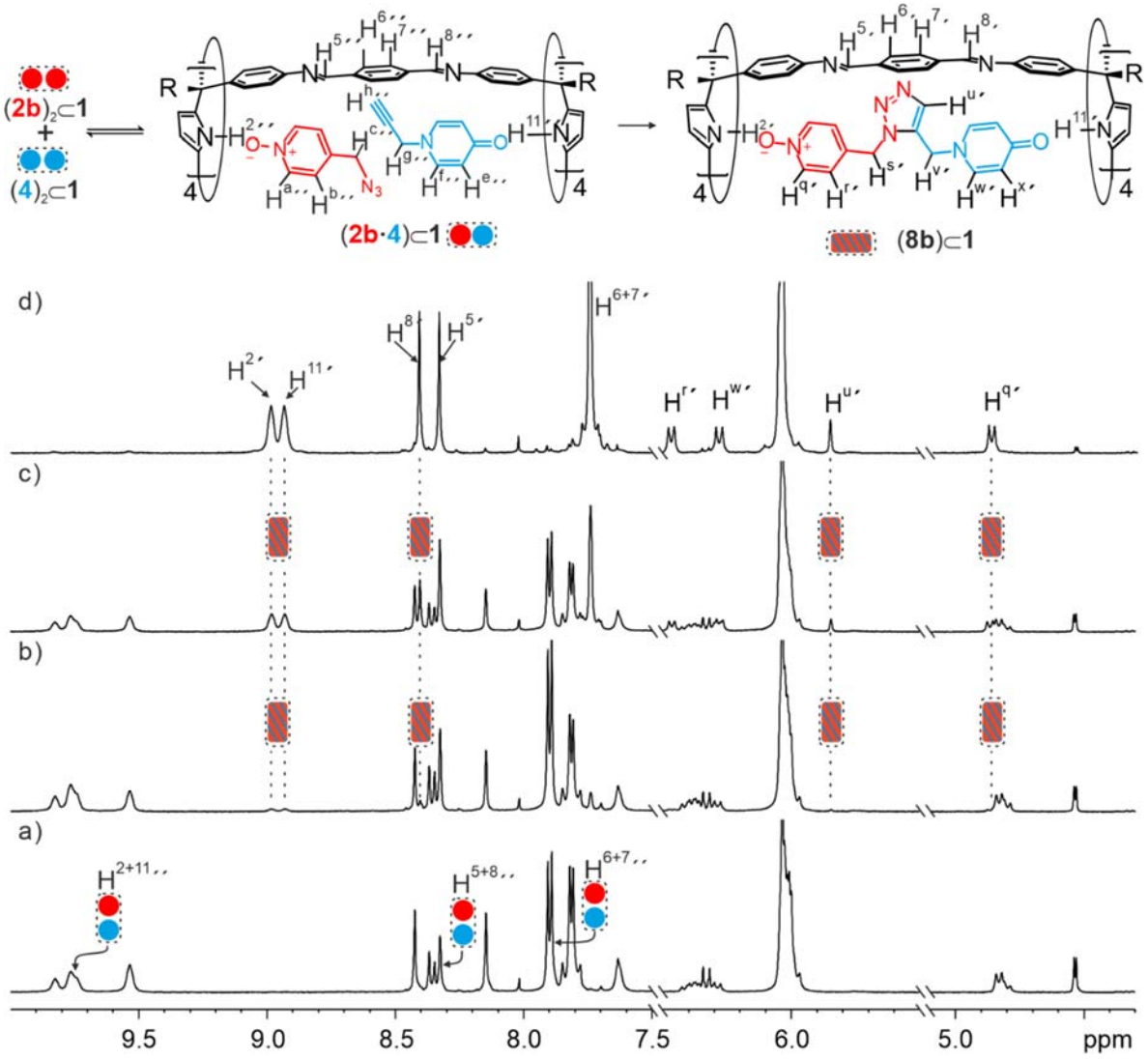


**Figure S 34.** Top) The 1,3-dipolar cycloaddition reaction between **2b** and **4** included in the octa-imine cage **1** yielded the complex **8b⊂1**. Bottom) Selected regions of the $^{1}$H NMR (300 MHz, 298 K, $CDCl_3$: $CD_3CN$ 9:1) spectra corresponding to the monitoring of the formation of complex **8b⊂1** starting from a 1:1:1 molar mixture of compounds **1**, **2b**, and **4**, respectively, after a) 0 h, b) 2 h, c) 24 h, and d) 312 h. Primed letters correspond to the proton signals in the 1:1 complexes, double-primed letters correspond to the 2:1 homo- and hetero-complexes.

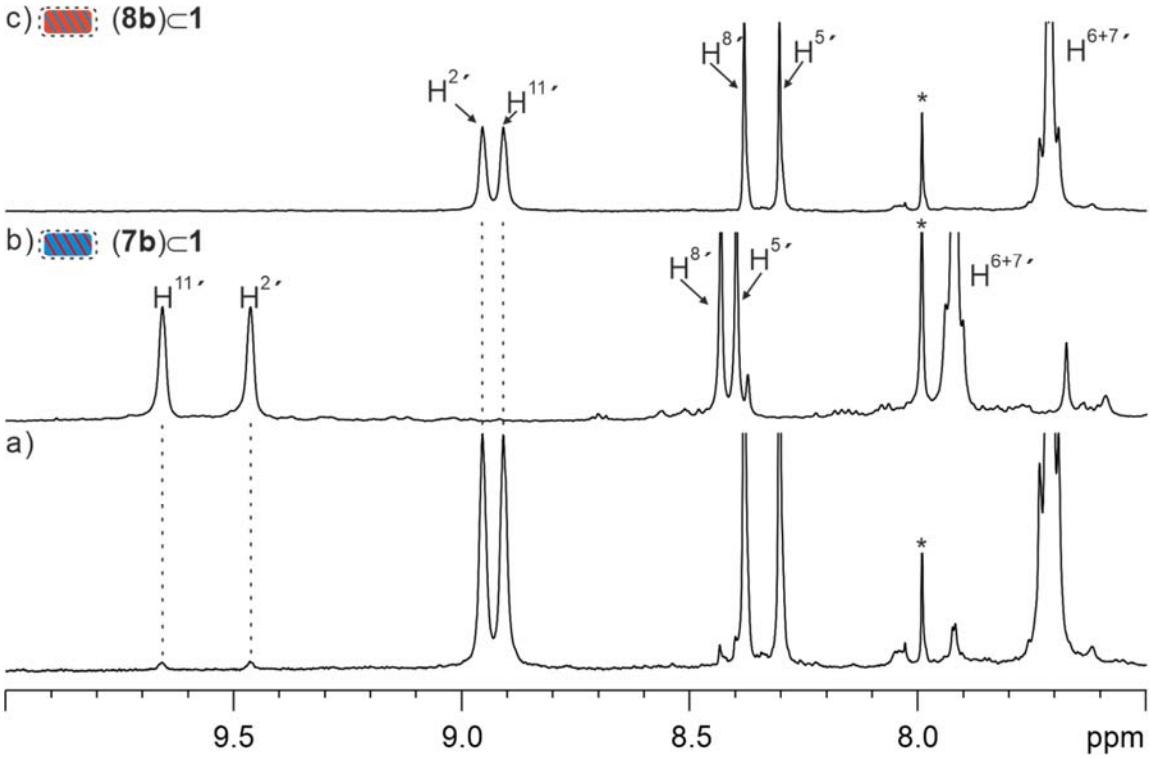


**Figure S 35.** a) Selected regions of the $^{1}$H NMR (300 MHz, 298 K, $CDCl_3$:$CD_3CN$ 9:1) spectra corresponding to the monitoring of the formation of complexes **8b⊂1** and **7b⊂1** starting from a 1:1:1 molar mixture of compounds **1**, **2b**, and **4** after 312 h. Spectrum b) and c) correspond to the **7b⊂1** and **8b⊂1** in the same solvent mixture, respectively. *Residual peak related to the excess of terephthaldehyde linker in the cage synthesis process.

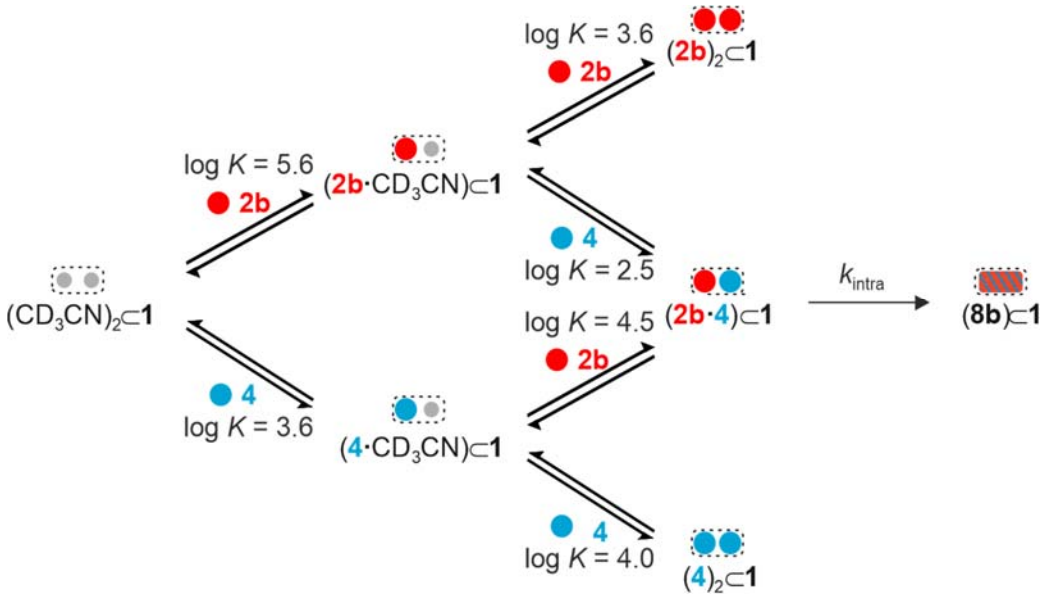


**Figure S 36.** Theoretical kinetic model used for the non-linear analysis of the experimental data including the values for the thermodynamic equilibrium constants determined/estimated for each binding process. Red spheres correspond to azido(methyl) pyridine-*N*-oxide **2b**; blue spheres correspond to 1-(2-propynyl)-4-pyridinone **4**; the dashed red-blue cylinder corresponds to the cycloaddition product **8b**.

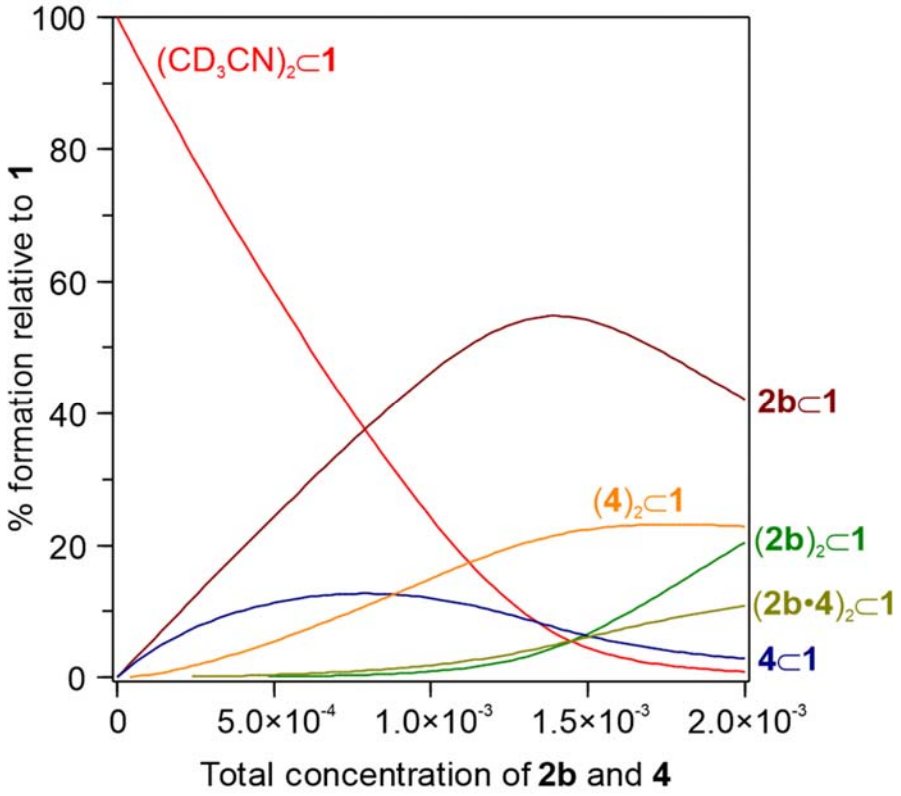


**Figure S 37.** Simulated speciation profile for octa-imine cage **1** (2 mM) with incremental amounts of **2b** (up to 2 mM) and **4** (up to 2 mM) determined using Hyperquad Simulation and Speciation (HySS2009) software using a model that considers the reversible formation of 1:1 and 2:1 homo- and hetero-inclusion complexes with the constants depicted in **Figure S 36**.

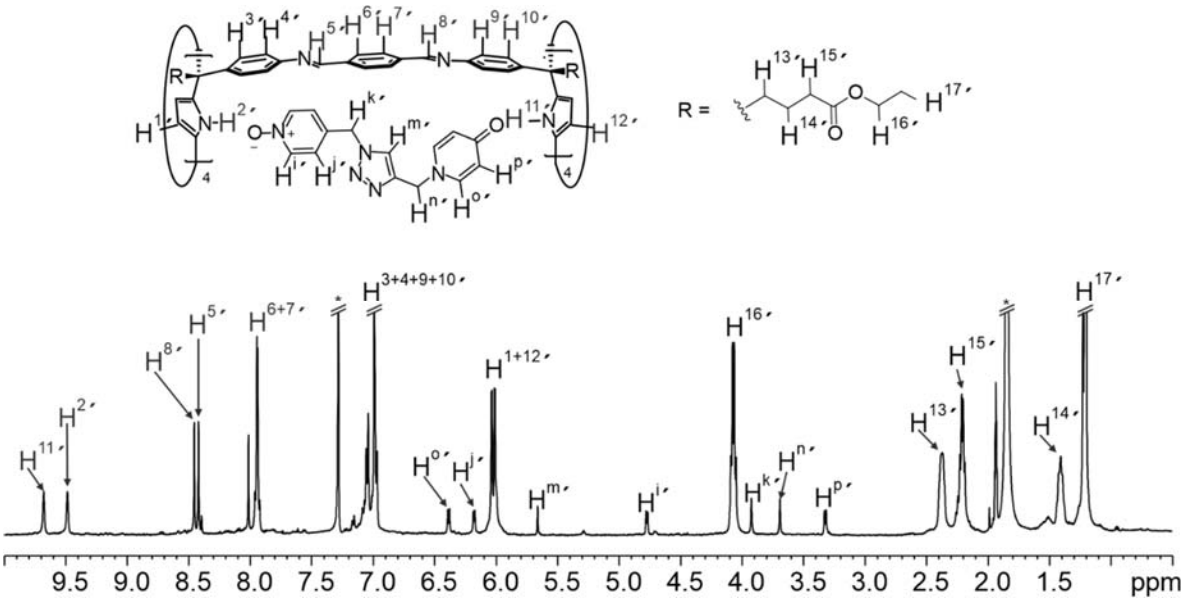


**Figure S 38.** $^{1}$H NMR spectrum (500 MHz, 298 K, $CDCl_3$:$CD_3CN$ 9:1) of **7b**⊂1 complex obtained from a solid-liquid extraction of the insoluble guest **7b** with a solution of $(CD_3CN)_2$⊂**1**.

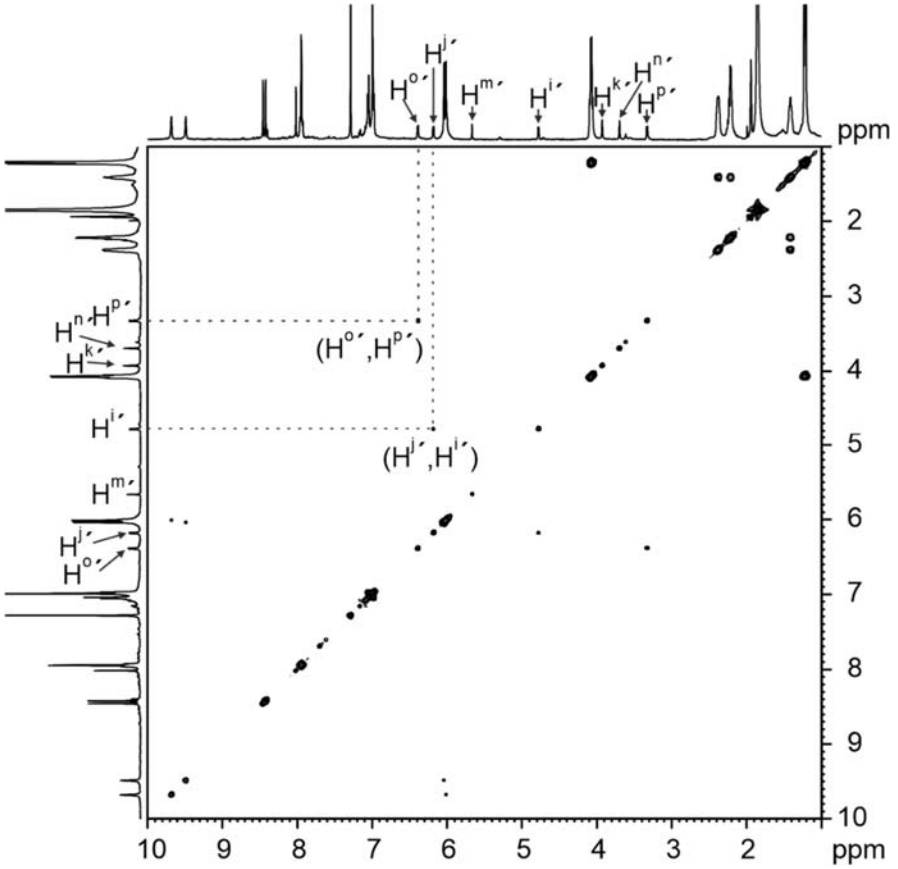


**Figure S 39.** Selected region of the $^{1}$H-$^{1}$H COSY NMR (500 MHz, at 298 K, $CDCl_3$: $CD_3CN$ 9:1) of **7b⊂1** complex.

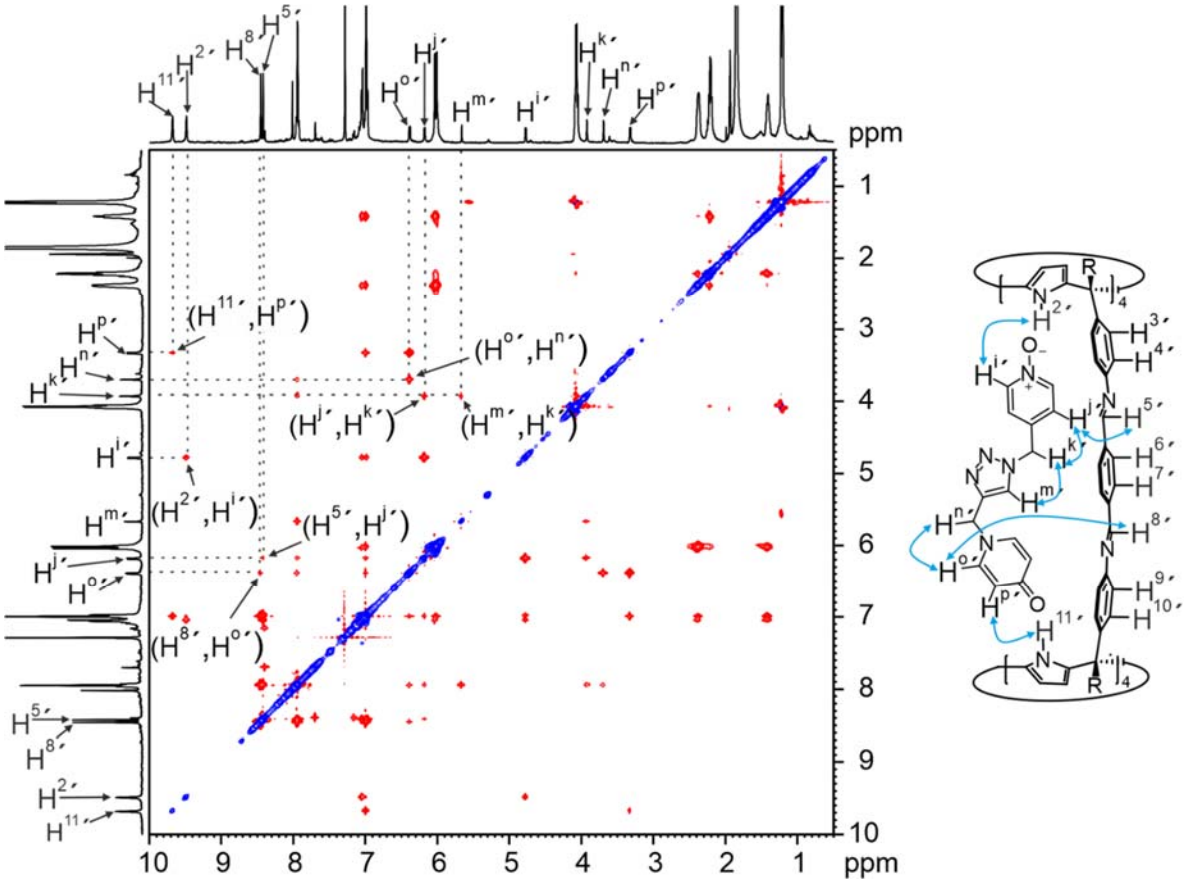


**Figure S 40.** Selected region of the $^{1}$H-$^{1}$H ROESY NMR (500 MHz, at 298 K, $CDCl_3$: $CD_3CN$ 9:1, D8 = 0.30 s) of **7b⊂1** complex.

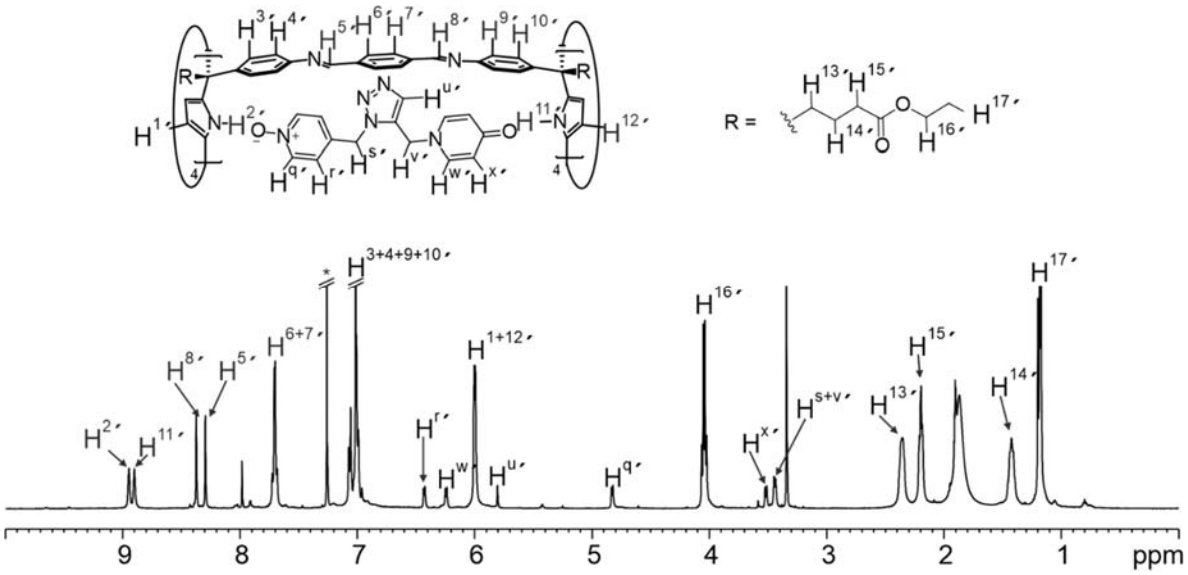


**Figure S 41.** $^{1}$H NMR spectrum (500 MHz, 298 K, $CDCl_3$:$CD_3CN$ 9:1) of **8b**⊂1 complex obtained from a filtrated solution of a solid-liquid extraction of the insoluble guest **8b** with a solution of $(CD_3CN)_2$⊂**1** in $CDCl_3$:$CD_3CN$ 9:1.

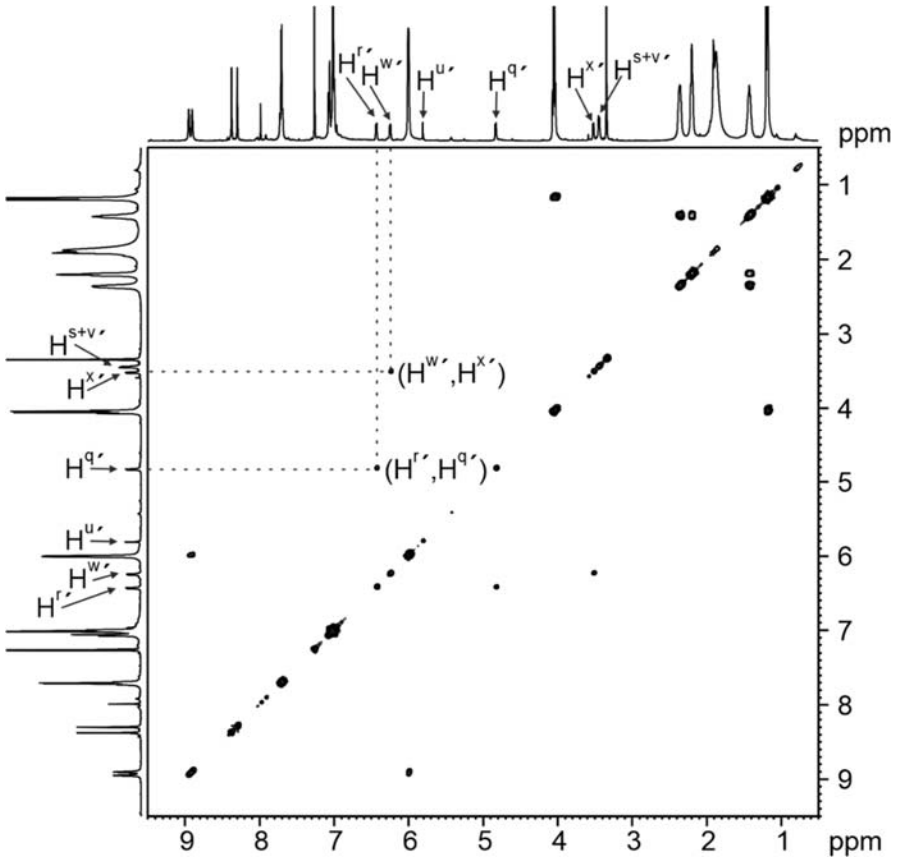


**Figure S 42.** Selected region of the $^{1}$H-$^{1}$H COSY NMR (500 MHz, at 298 K, $CDCl_3$: $CD_3CN$ 9:1) of **8b**⊂**1** complex.

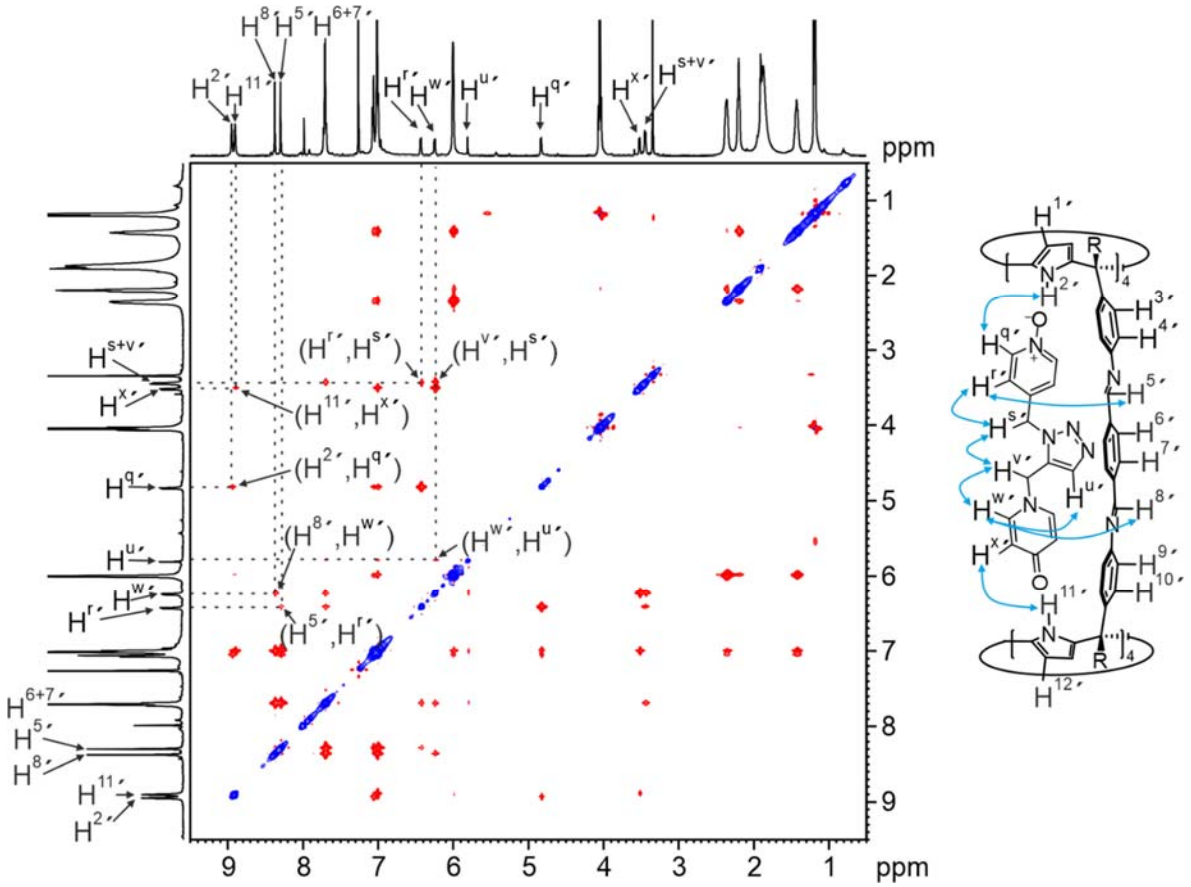


**Figure S 43.** Selected region of the $^{1}$H-$^{1}$H ROESY NMR (500 MHz, at 298 K, $CDCl_3$: $CD_3CN$ 9:1, D8 = 0.30 s) of **8b⊂1** complex.

### 3.4. Co-inclusion of 4-azido(ethyl) pyridine-*N*-oxide 2c and 1-(2-propynyl)-4-pyridinone 4 in 1.

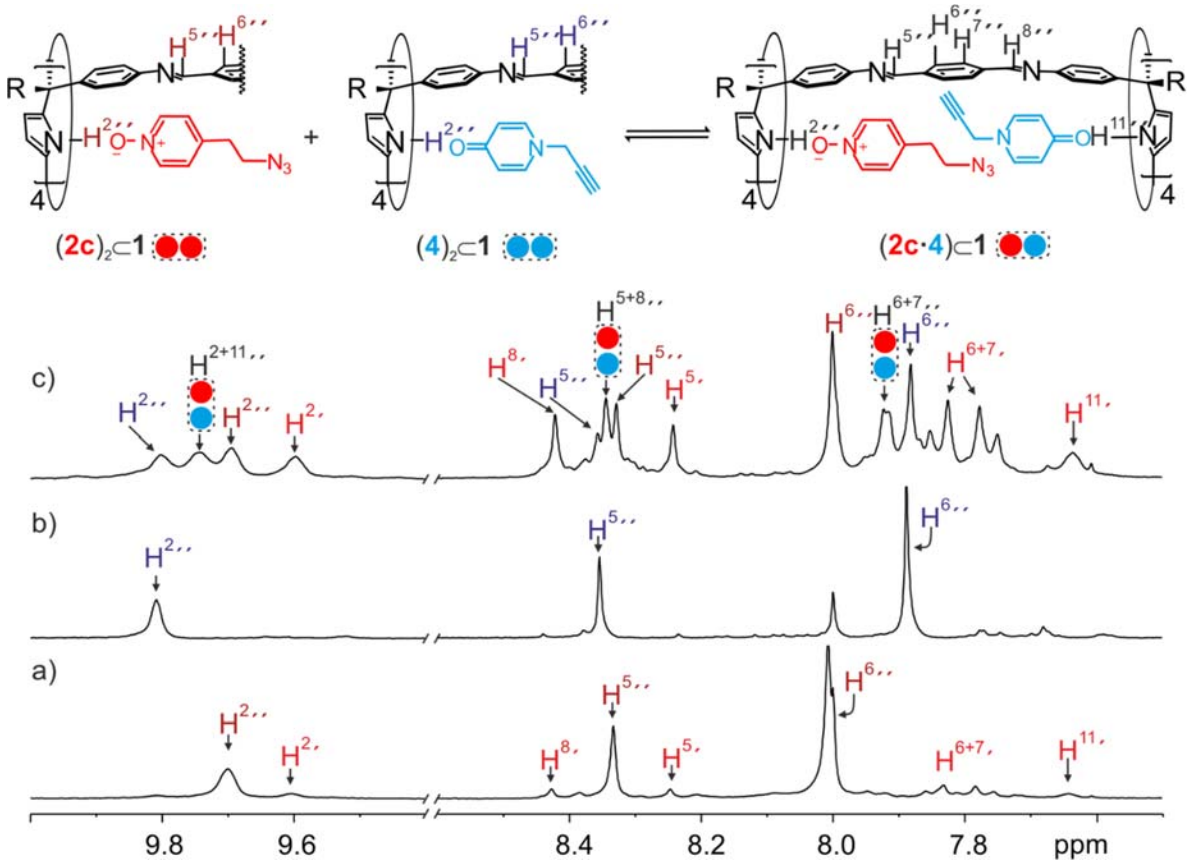


**Figure S 44.** Selected regions of $^{1}$H NMR (400 MHz, 298K, $CDCl_3$:$CD_3CN$ 9:1) spectra of solutions containing: a) 1:1.5 mixture of cage **1** and **2c**; b) 1:2 mixture of cage **1** and **4**; and c) 1:1:1 mixture of **1**:**2c**:**4**. Primed and double-primed protons correspond to the 1:1 and 2:1 complexes, respectively. Proton assignments in red correspond to complexes with **2c** included, and proton assignments in blue correspond to complexes with **4** included.

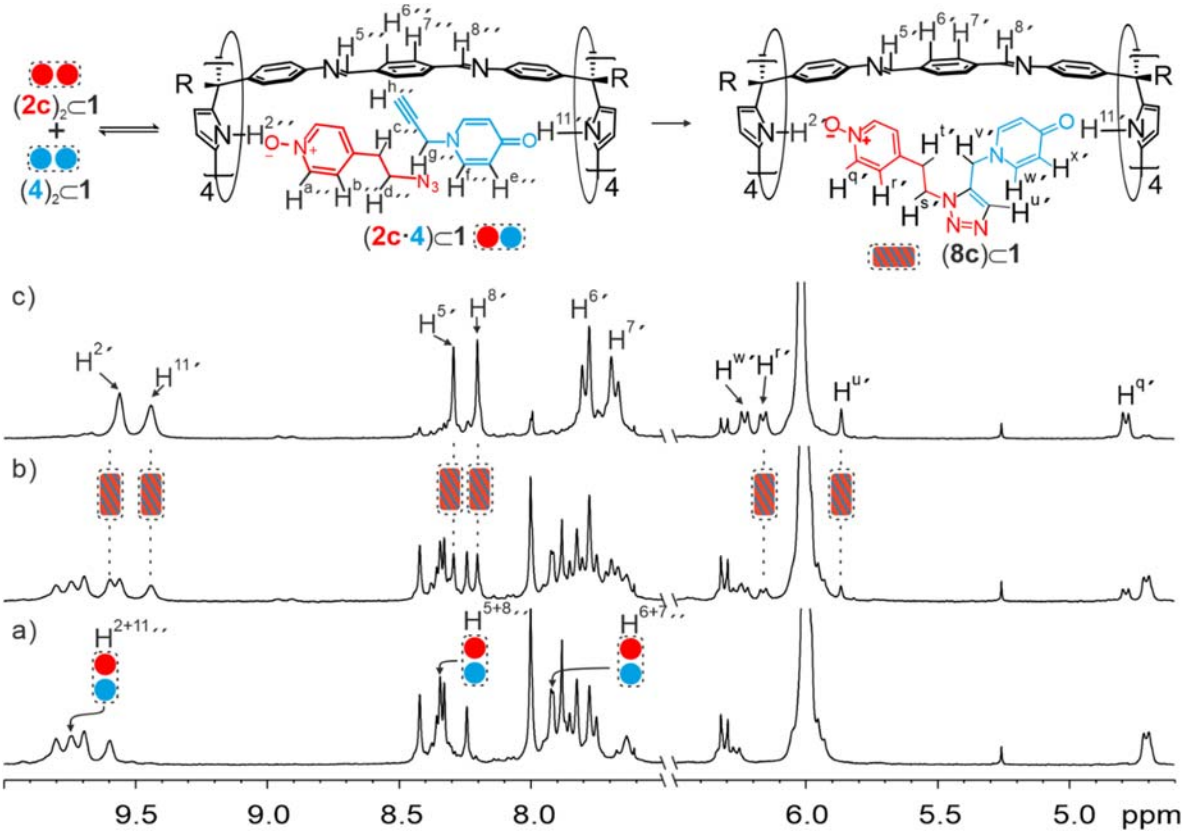


**Figure S 45.** Top) The 1,3-dipolar cycloaddition reaction between **2c** and **4** included in the octa-imine cage **1** yielded the complex **8c⊂1**. Bottom) Selected regions of the $^{1}$H NMR (300 MHz, 298 K, $CDCl_3$:$CD_3CN$ 9:1) spectra corresponding to the monitoring of the formation of complex **8c⊂1** starting from a 1:1:1 molar mixture of compounds **1**, **2c**, and **4**, respectively, after a) 0 h, b) 96 h. Spectrum c) corresponds to the **8c⊂1** in the same solvent mixture. Primed and double-primed protons correspond to the proton signals of the 1:1 and 2:1 homo- and hetero-complexes, respectively.

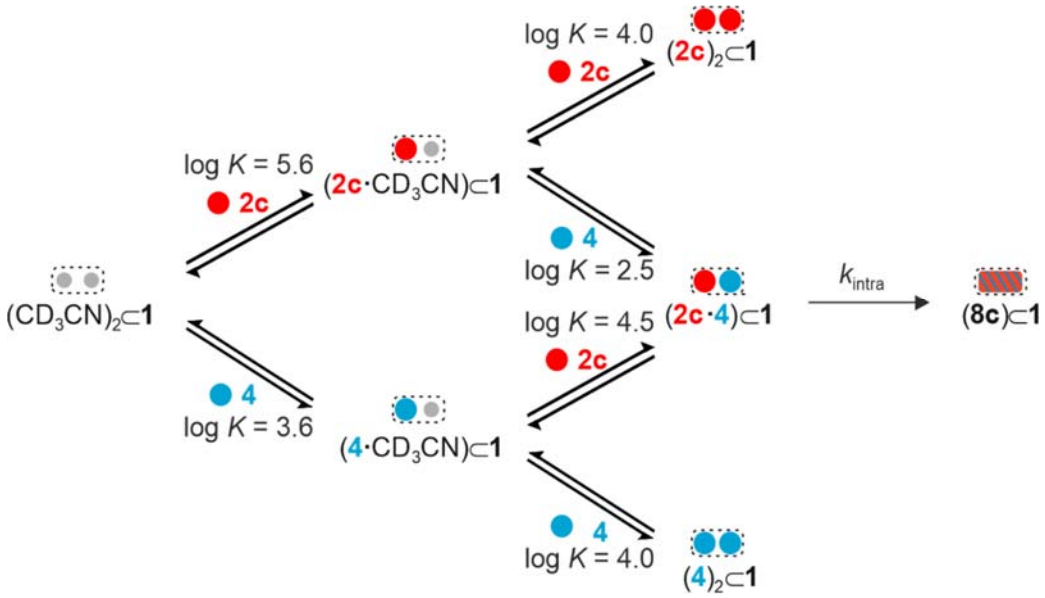


**Figure S 46.** Theoretical kinetic model used for the non-linear analysis of the experimental data including the values for the thermodynamic equilibrium constants determined/estimated for each binding process. Red spheres correspond to azido(ethyl) pyridine-*N*-oxide **2c**; blue spheres correspond to 1-(2-propynyl)-4-pyridinone **4**; and red-blue dashed cylinder correspond to the cycloaddition product **8c.**

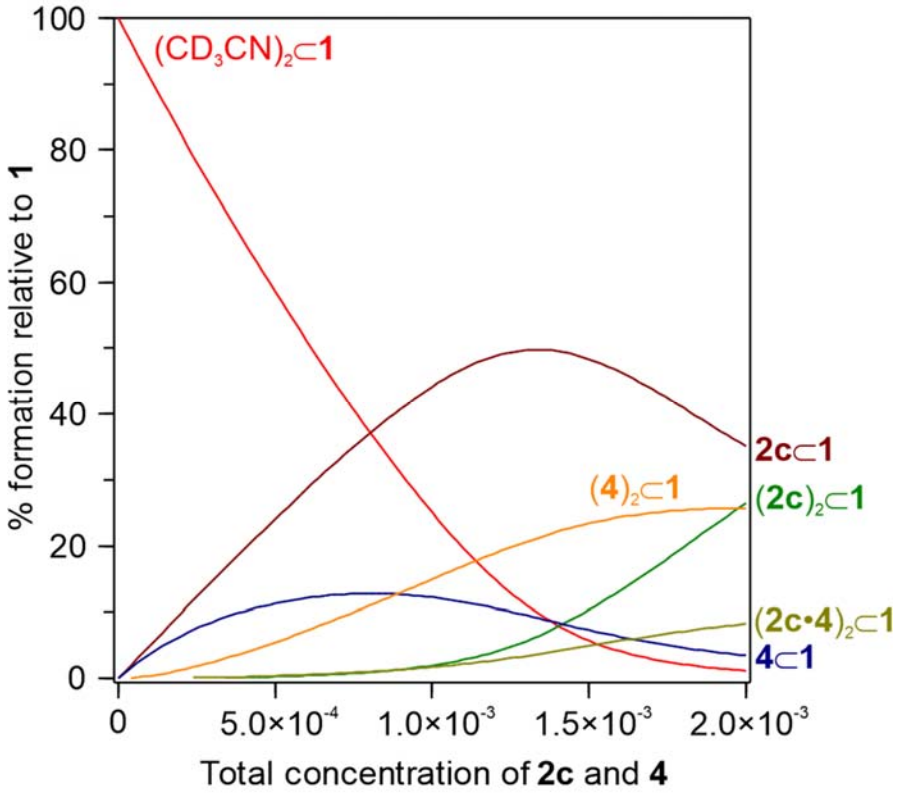


**Figure S 47.** Simulated speciation profile for octa-imine cage **1** (2 mM) with incremental amounts of **2c** (up to 2 mM) and **4** (up to 2 mM) determined using Hyperquad Simulation and Speciation (HySS2009) software using a model that considers the reversible formation of 1:1 and 2:1 homo- and hetero-inclusion complexes with the constants depicted in **Figure S 46**.

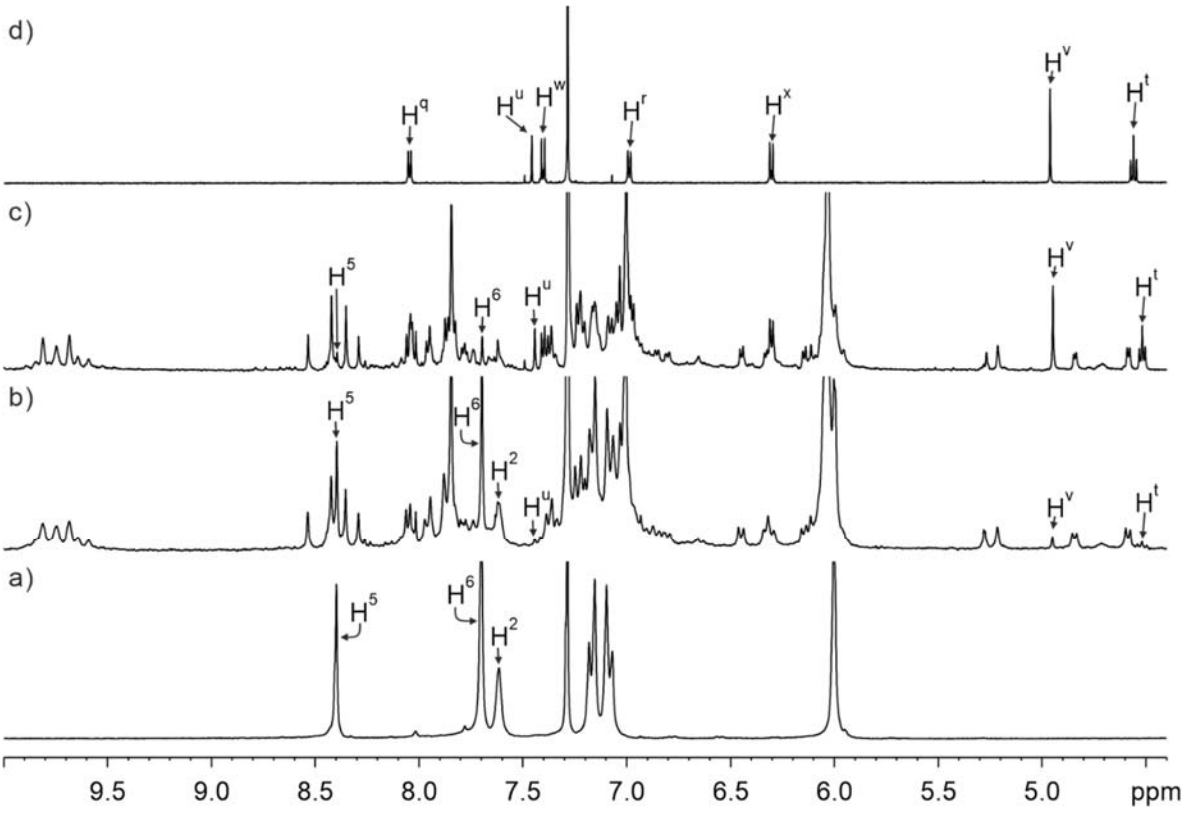


**Figure S 48.** Selected regions of the $^1$H NMR (400 MHz, 298 K, $CDCl_3$:$CD_3CN$ 9:1) spectra of the titration of a 2 mM solution of octa-imine cage **1**, upon addition of a) 0 equiv., b) 1 equiv., c) 2 equiv. of **7c**. Spectrum d) corresponds to the free **7c** in the same solvent mixture.

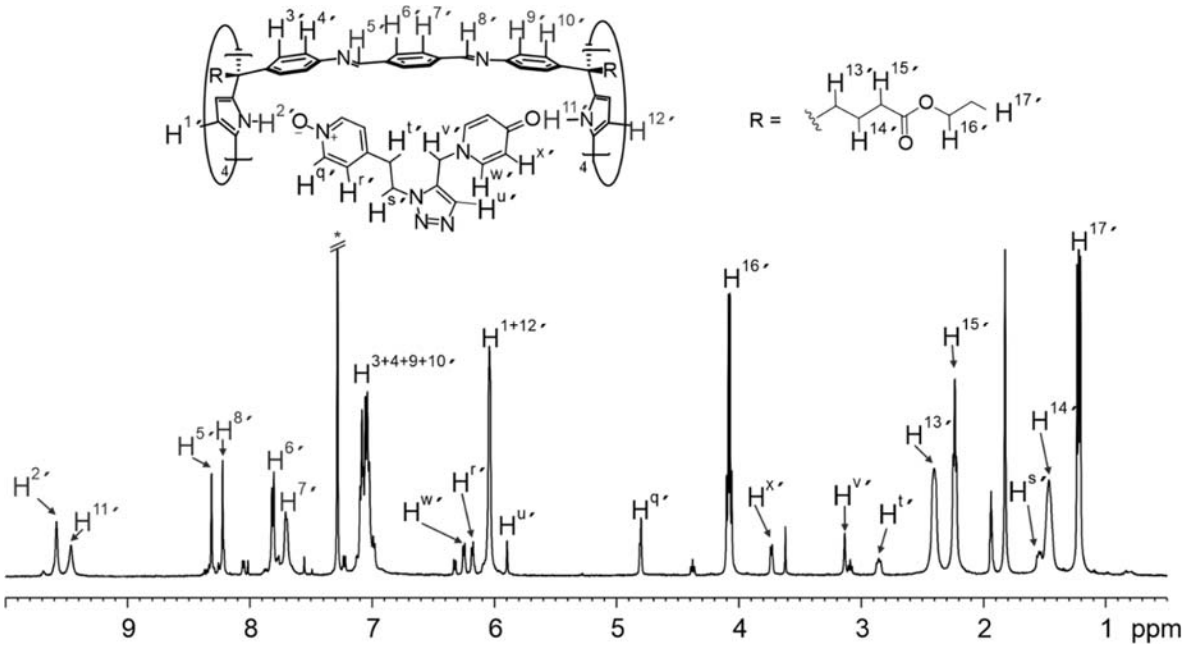


**Figure S 49.** $^{1}$H NMR spectrum (500 MHz, 298 K, $CDCl_3$:$CD_3CN$ 9:1) of **8c**⊂1 complex obtained from a filtered solution of a solid-liquid extraction of the insoluble guest **8c** with a solution of $(CD_3CN)_2$⊂**1**.

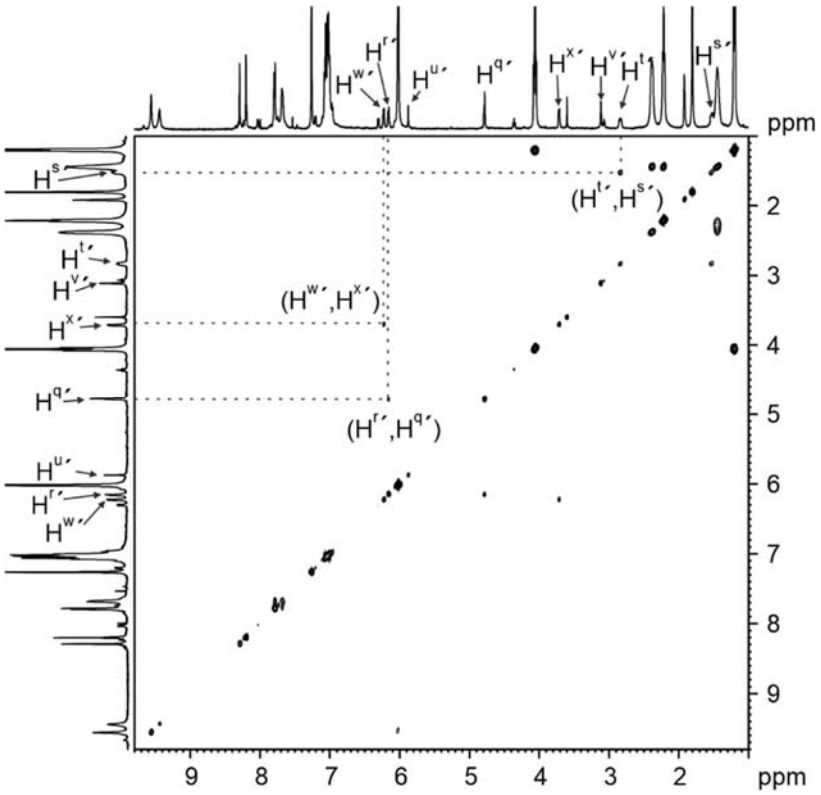


**Figure S 50.** Selected region of the $^{1}$H-$^{1}$H COSY NMR (500 MHz, at 298 K, $CDCl_3$: $CD_3CN$ 9:1) of **8c⊂1** complex.

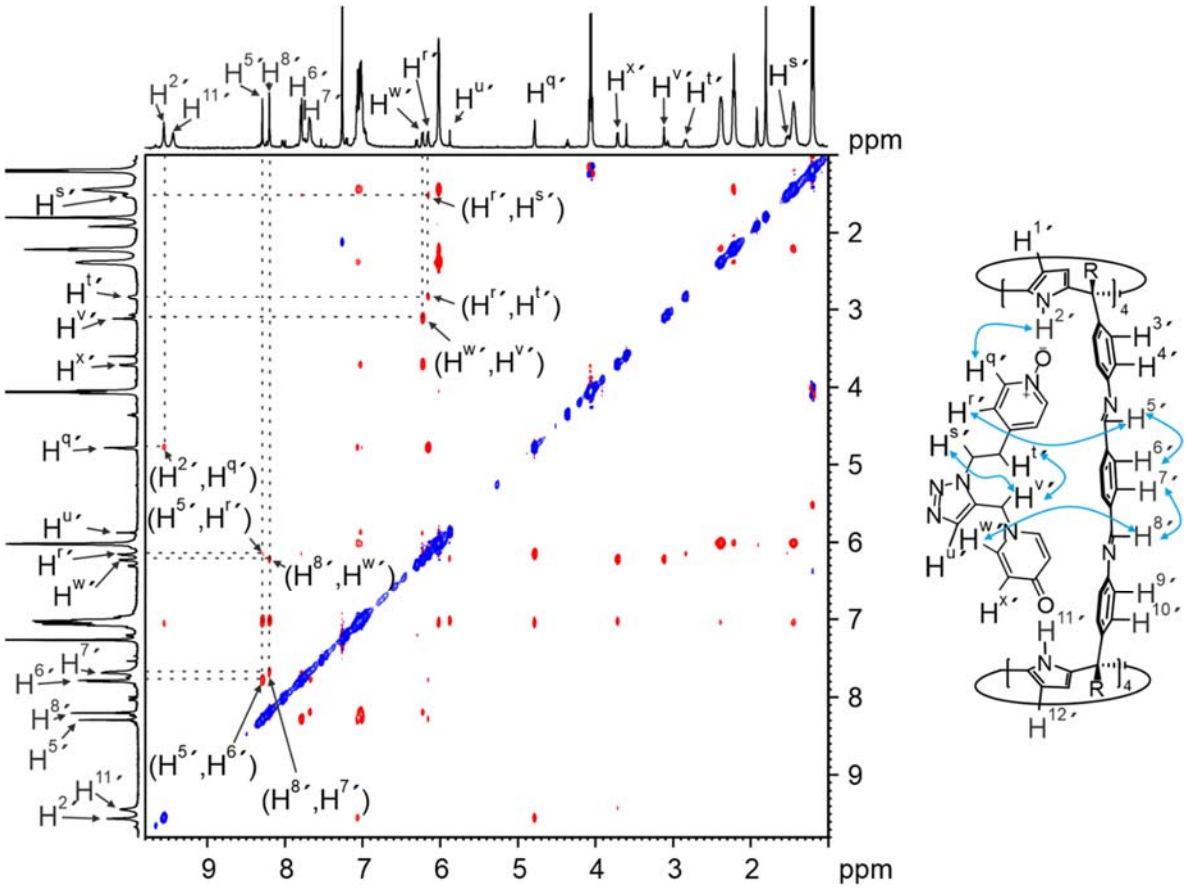


**Figure S 51.** Selected region of the $^{1}$H-$^{1}$H ROESY NMR (500 MHz, at 298 K, $CDCl_3$: $CD_3CN$ 9:1, D8 = 0.30 s) of **8c⊂1** complex.

### 3.5. Isothermal Titration Calorimetry experiments.

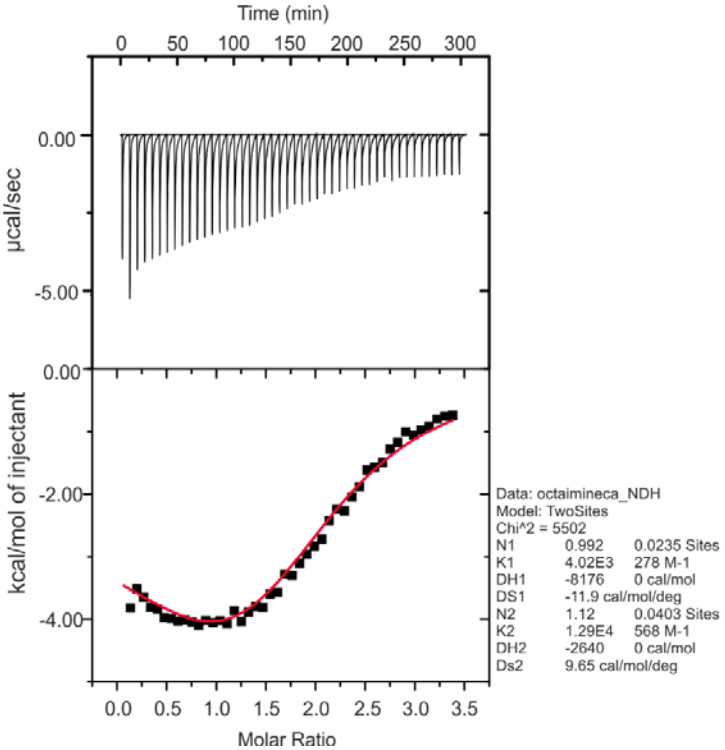


**Figure S 52.** Top- Traces of the raw data (heat vs time) of the ITC experiment of cage **1** ([cell] = $1 \times 10^{-3}$ M) with **4** ([syringe]= $2.0 \times 10^{-2}$ M). The solutions were prepared using a chloroform: acetonitrile 9:1 solvent mixture. Bottom- Normalized integrated heat (black squares) vs. **4**/**1** molar ratio. Experimental data were fit to a "two-binding sites" model (red line).

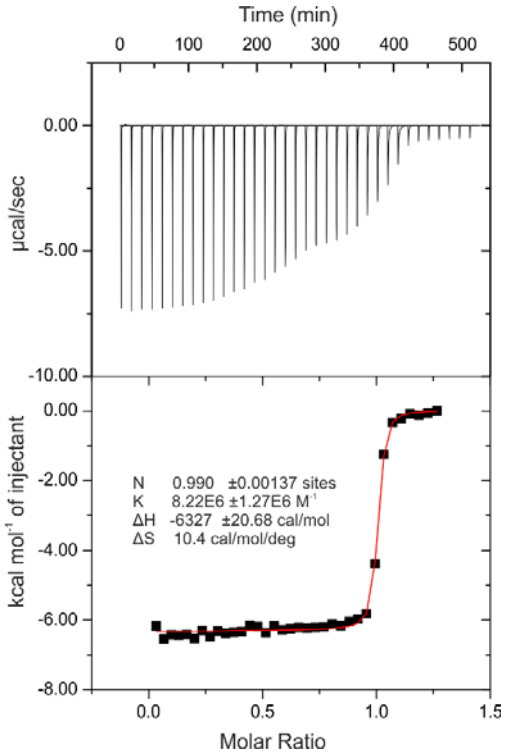


**Figure S 53.** Top- Traces of the raw data (heat vs time) of the ITC experiment of **7a** ([cell] = 6.4 × $10^{-4}$ M) with cage **1** ([syringe] =3.7 × $10^{-3}$ M). The solutions were prepared using a chloroform: acetonitrile 9:1 solvent mixture. Bottom- Normalized integrated heat (black squares) vs. **1**/**7a** molar ratio. The experimental data were fit to one set of sites binding model (red line).

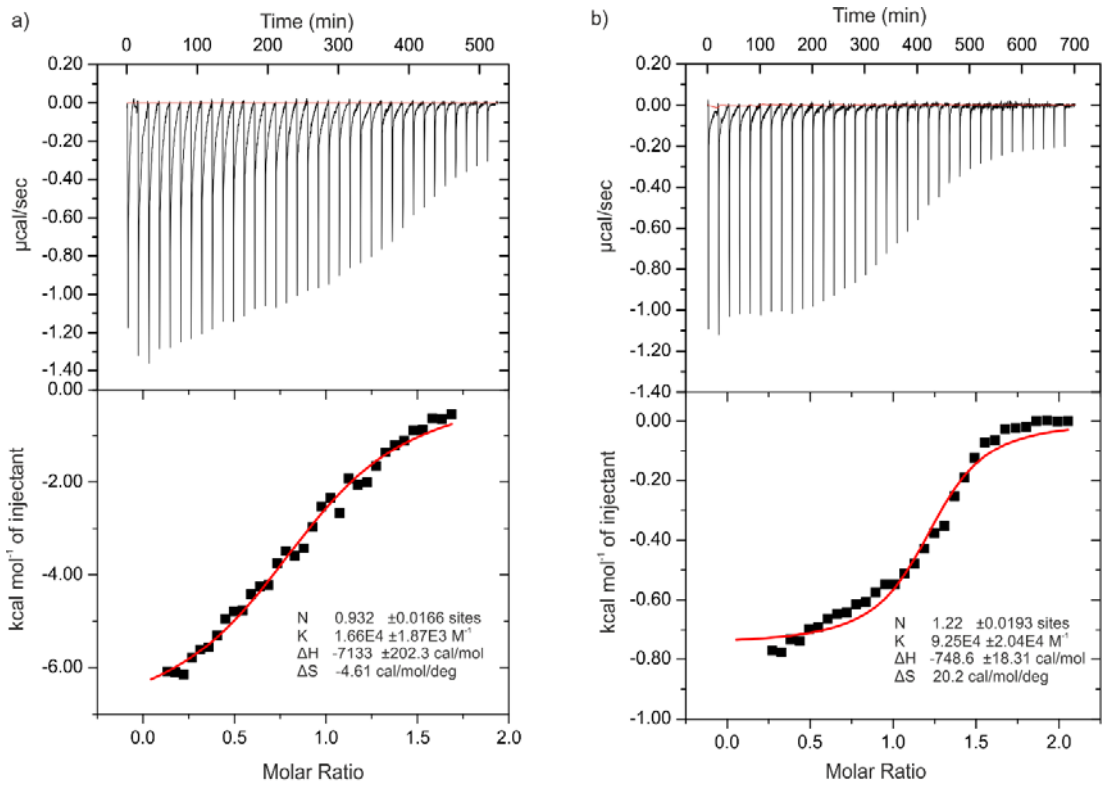


**Figure S 54.** Top- Traces of the raw data (heat vs time) of the ITC experiment of **7b** (a) ([cell] = $4.8 \times 10^{-4}$ M) and **8b** (b) ([cell] = $4.8 \times 10^{-4}$ M) with cage 1 ([syringe] =$3.7 \times 10^{-3}$ M). The solutions were prepared using a chloroform: acetonitrile 9:1 solvent mixture. Bottom- Normalized integrated heat (black squares) vs. **1**/**7b** (a) and **1**/**8b** (b) molar ratio. The experimental data were fit to one-set-of-sites binding model (red line).

To further support the ITC results, we conducted a competitive binding experiment between **7b** and **8b** with cage **1**. First, we prepared an equimolar solution of **7b** and **8b** in methanol-$d_4$. After removing the methanol-$d_4$ under vacuum, we added 1 equiv. of cage **1**, dissolved in a $CDCl_3$:$CD_3CN$ 9:1 solvent mixture, to the resulting solid residue. This produced a suspension, which was sonicated before NMR spectroscopy analysis. The initial $^1$H NMR spectrum revealed two sets of signals corresponding to the protons of octa-imine cage, which were assigned to the complexes **7b⊂1** and **8b⊂1**. The integrals of selected proton signals at t = 60 min assigned that the molar ratio of the complexes **7b⊂1**:**8b⊂1** was 77:23. The initially higher proportion of the **7b⊂1** complex may be attributed to the superior solubility of **7b** or/and a more favorable kinetic pathway for the formation of the **7b⊂1** complex. We monitored the mixture by $^1$H NMR spectroscopy for 10 days. We observed the gradual increase of the proton signals assigned to the **8b⊂1** complex at the expense of those of the **7b⊂1** counterpart. After 12 days, integration of the NH signals indicated a **7b⊂1**:**8b⊂1** ratio close to 50:50. Using COPASI to simulate the kinetics of the exchange, we extrapolated that the system would reach equilibrium after approximately six

months, yielding a final **7b⊂1**:**8b⊂1** ratio of 25:75. This is consistent with the 3:97 ratio obtained in the kinetic experiment of the included reaction, which reflects the energy difference between the two transition states.

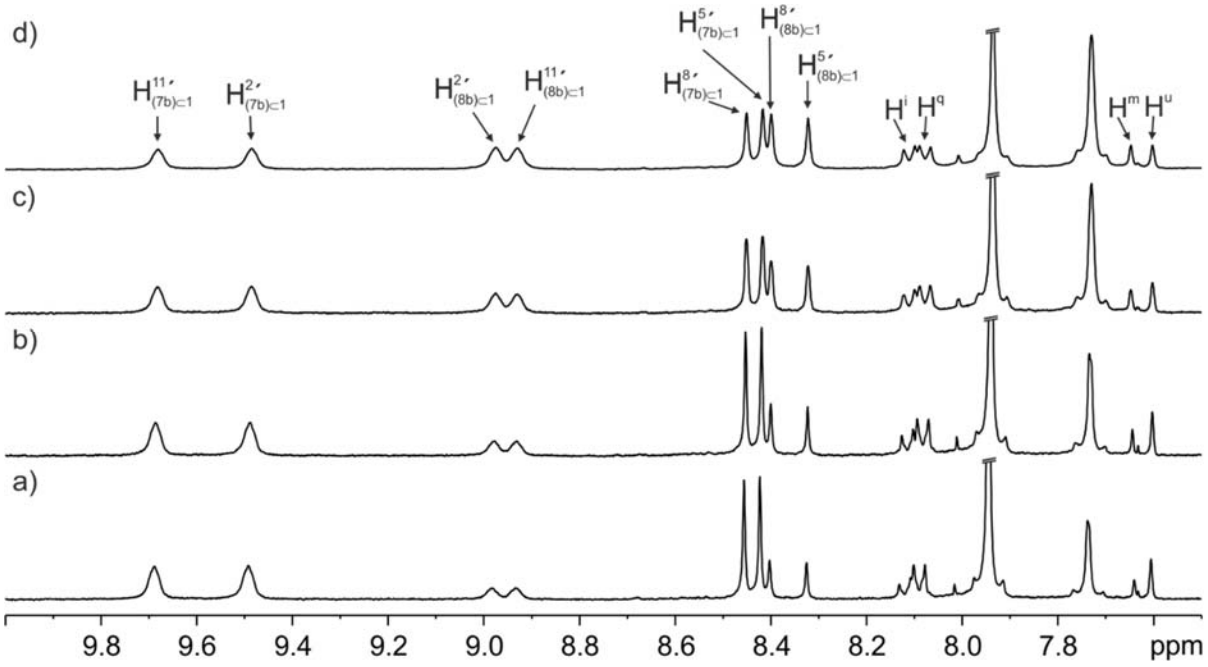


**Figure S 55.** Selected region of the $^{1}$H NMR spectra acquired over time in the competitive binding experiment between **7b** and **8b** with cage **1**: a) 1h; b) 96 h; c) 192 h; d) 288h.

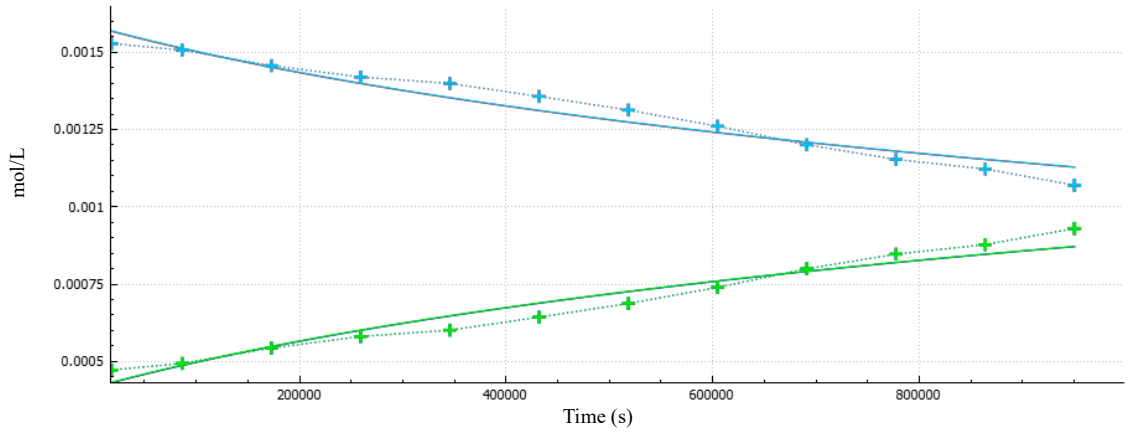


**Figure S 56.** Plot of the changes in the concentrations of the two complexes **7b⊂1** (green crosses connected by dotted line) and **8b⊂1** (blue crosses connected by a dotted line) monitored with time (seconds) using $^{1}$H NMR spectroscopy. Fit (COPASI) of the experimental data to a kinetic model considering the competitive binding between **7b** and **8b** with cage **1** to produce the two complexes (continuous green and blue lines, respectively).

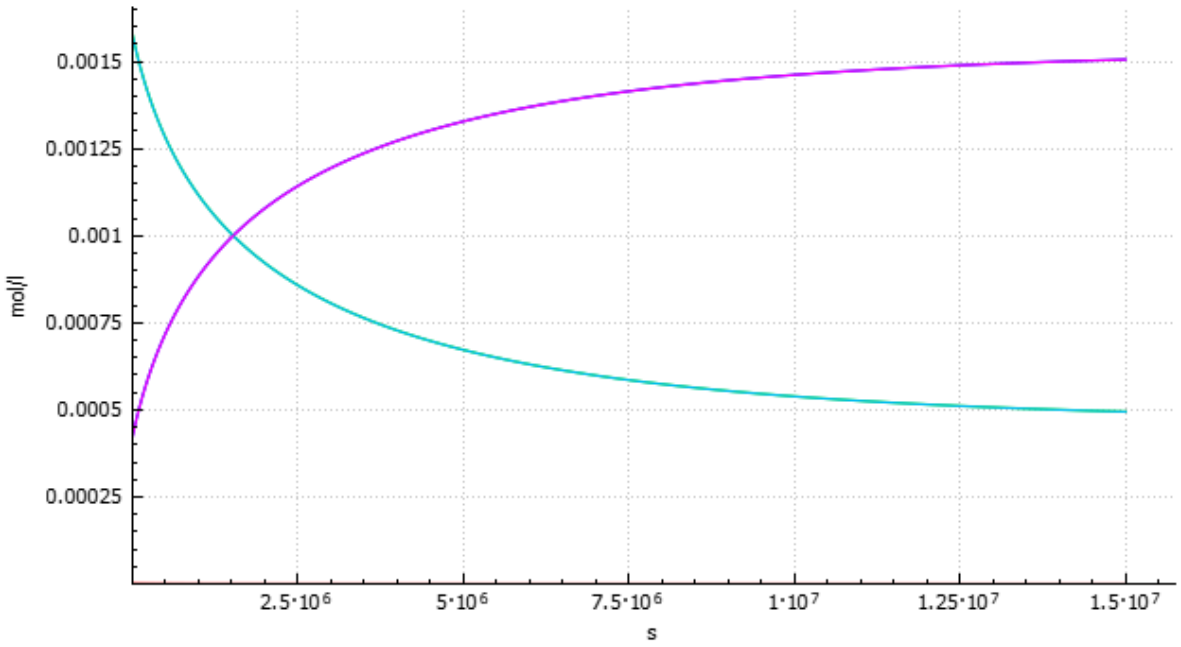


**Figure S 57.** Simulated time course (COPASI) of the competitive binding experiment between **7b** (blue line) and **8b** (purple line) with cage **1** at equimolar mM concentrations to extrapolate the composition of the mixture at equilibrium (six months) to be **7b⊂1:8b⊂1** = 25:75. The value of the kinetics constants used for the two considered reversible and competitive reactions were those obtained from the fit shown in the previous figure.

## 4. Kinetic characterization of cycloaddition reaction

### 4.1. Cycloaddition reactions of 2a-2c with 4 in octa-imine cage 1.

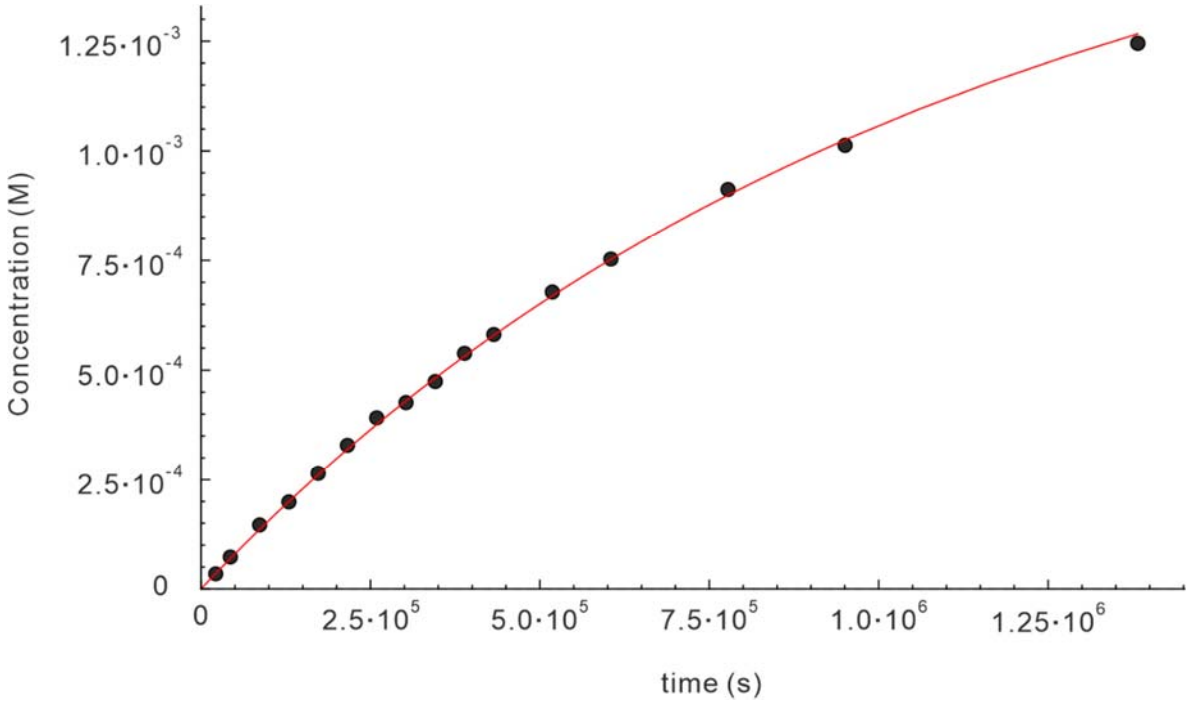


**Figure S 58.** Changes in the concentration of **7a⊂1** complex (black dots) with time starting from a 1:1:1 mixture of **1**, **2a**, and **4**, respectively, in $CDCl_3$:$CD_3CN$ 9:1. The solid red line represents the fit of the experimental kinetic data to the theoretical model using the parameters estimation module of COPASI software Version 4.25. The $k_{on}/k_{off}$ ratios of all binding equilibria were manually fixed based on the determined binding constants. $k_{intra}$ was the only variable parameter used for the fit and returned a value of $k_{intra} = 4.4 \pm 0.8 \times 10^{-6}$ $s^{-1}$. Error-values are reported as standard deviations from two separate kinetic experiments.

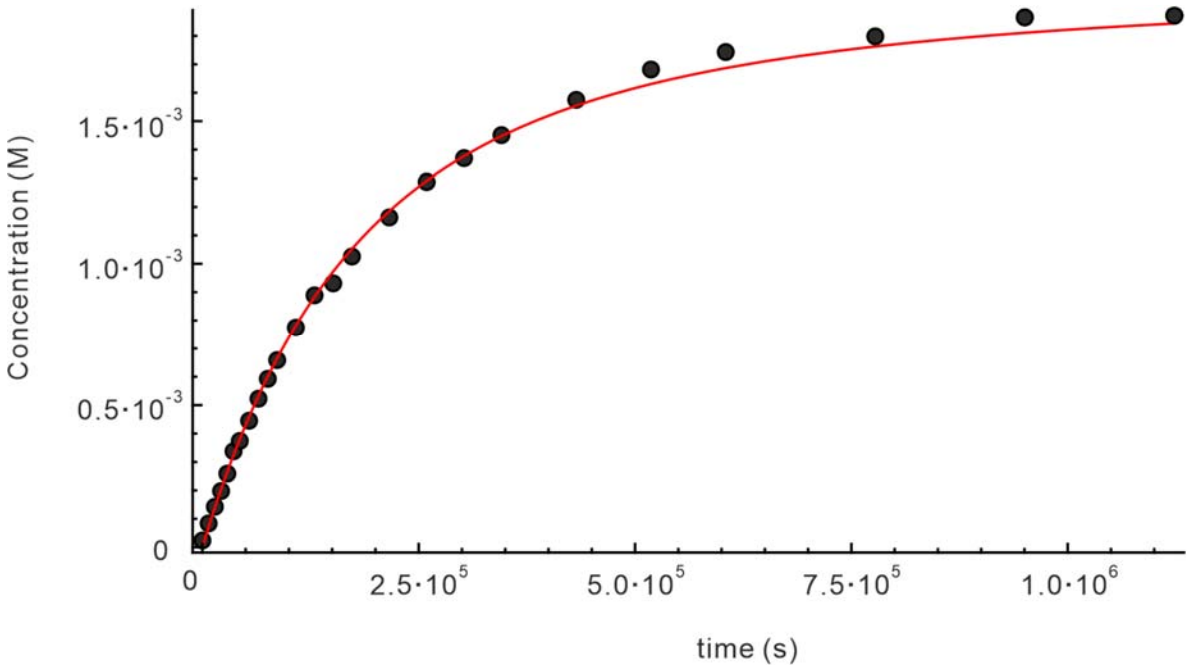


**Figure S 59.** Changes in the concentration of **8b⊂1** complex (black dots) with time starting from a 1:1:1 mixture of **1**, **2b**, and **4**, respectively, in $CDCl_3$:$CD_3CN$ 9:1. The solid red line represents the fit of the experimental kinetic data to the theoretical model using the parameters estimation module of COPASI software Version 4.25. The $k_{on}/k_{off}$ ratios of all binding equilibria were manually fixed based on the determined binding constants. $k_{intra}$ was the only variable parameter used for the fit and returned a value of $k_{intra} = 5.1 \pm 0.4 \times 10^{-5}$ $s^{-1}$. Error-values are reported as standard deviations from two separate kinetic experiments.

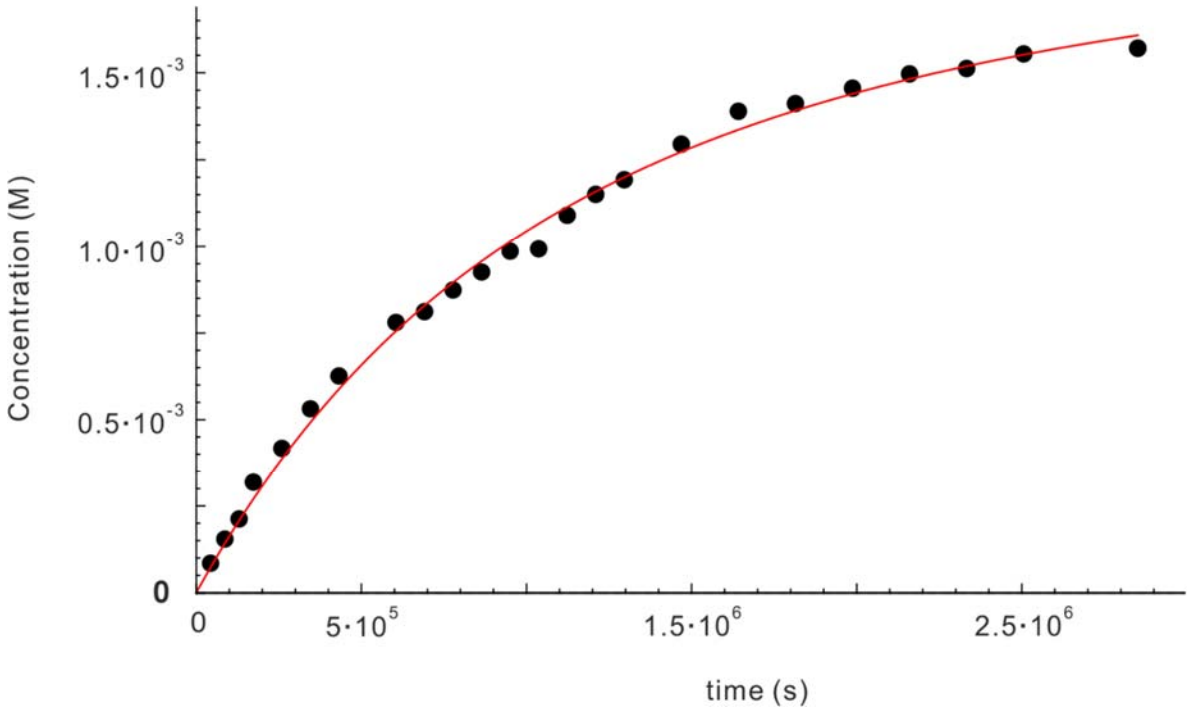


**Figure S 60.** Changes in the concentration of **8c⊂1** complex (black dots) with time starting from a 1:1:1 mixture of **1**, **2c**, and **4**, respectively, in $CDCl_3$:$CD_3CN$ 9:1. The solid red line represents the fit of the experimental kinetic data to the theoretical model using the parameters estimation module of COPASI software Version 4.25. The $k_{on}/k_{off}$ ratios of all binding equilibria were manually fixed based on the determined binding constants. $k_{intra}$ was the only variable parameter used for the fit and returned a value of $k_{intra} = 4.7 \pm 0.4 \times 10^{-6}$ $s^{-1}$. Error-values are reported as standard deviations from two separate kinetic experiments.

### 4.2.Cycloaddition reactions of 2a-2b with 4 in the bulk.

We carried out the cycloaddition reactions in the bulk in chloroform:acetonitrile 9:1 solvent mixture at 297 K. We used 4-methyl pyridine-*N*-oxide as the internal standard (i.s.), which exhibited a distinct retention time compared to reactants **2a-b** and **4**, as well as products **7a-b** and **8a-b**. Four different concentrations of **7a** (0.1, 0.05, 0.02, 0.01 mM) with the same concentration of i.s. (1 mM) were used for the calibration curve ($A_{product}/A_{i.s.}$) at 300 nm. Four different concentrations of **7b** and **8b** (0.1, 0.05, 0.02, 0.01 mM) with the same concentration of i.s. (0.1 mM) were used for calibration curve ($A_{product}/A_{i.s.}$) at 276 nm.

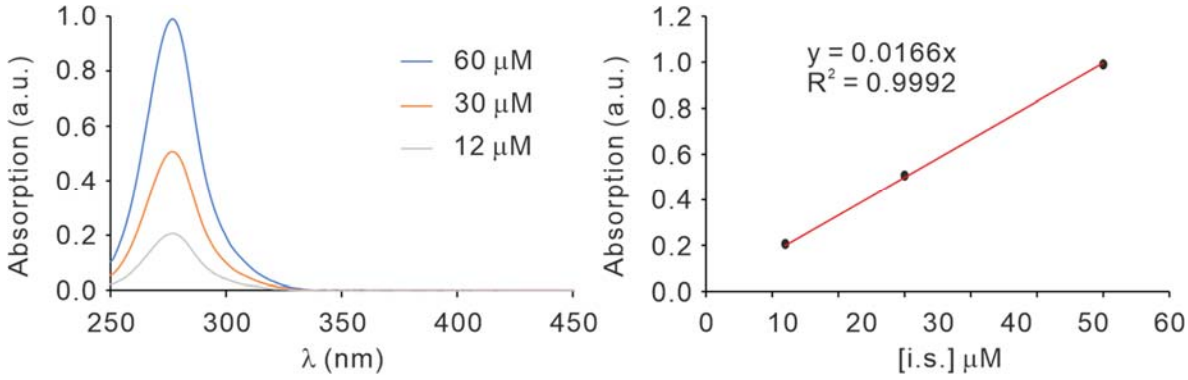


**Figure S 61.** Left- UV-vis absorption spectrum of 4-methyl pyridine-*N*-oxide (i.s.) with different concentrations ($\lambda_{max}$ = 277 nm). Right- Plot of the absorption change at 277 nm *vs.* concentration of 4-methyl pyridine-*N*-oxide. The slope of the red line corresponds to the extinction coefficient in $\lambda_{max}$ ($\varepsilon$ = 16600 $M^{-1}\cdot cm^{-1}$).

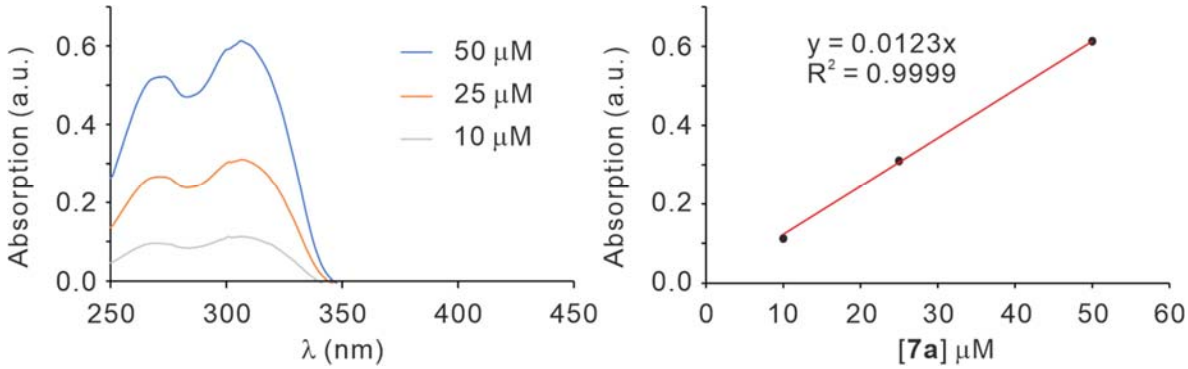


**Figure S 62.** Left- UV-vis absorption spectrum of **7a** with different concentrations ($\lambda_{max}$ = 300 nm). Right- Plot of the absorption change at 300 nm *vs.* concentration of **7a**. The slope of the red line corresponds to the extinction coefficient in $\lambda_{max}$ ($\varepsilon$ = 12300 $M^{-1}\cdot cm^{-1}$).

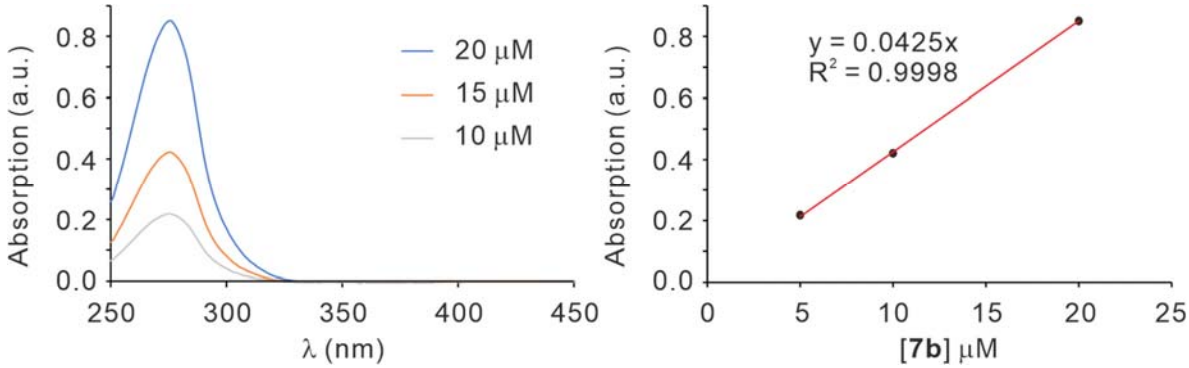


**Figure S 63.** Left- UV-vis absorption spectrum of **7b** with different concentrations ($\lambda_{max}$ = 276 nm). Right- Plot of the absorption change at 276 nm *vs.* concentration of **7b**. The slope of the red line corresponds to the extinction coefficient in $\lambda_{max}$ ($\varepsilon$ = 42500 $M^{-1}\cdot cm^{-1}$).

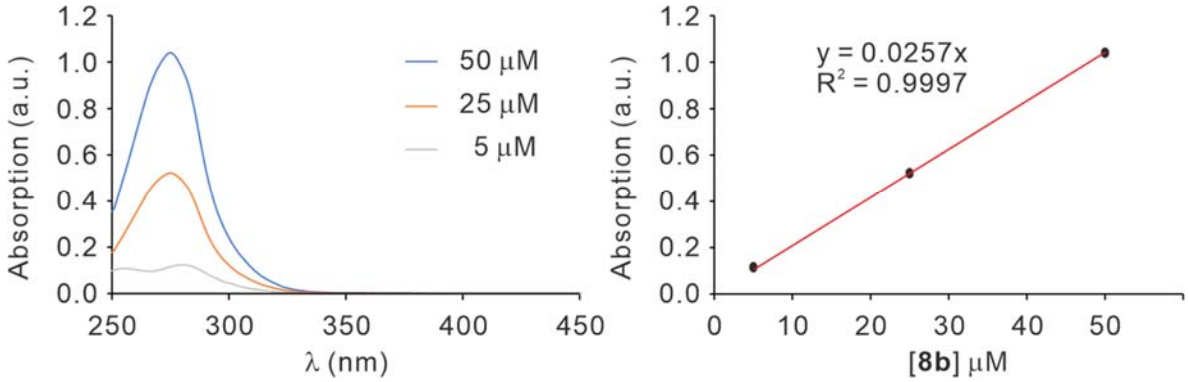


**Figure S 64.** Left- UV-vis absorption spectrum of **8b** with different concentrations ($\lambda_{max}$ = 276 nm). Right- Plot of the absorption change at 276 nm vs. concentration of **8b**. The slope of the red line corresponds to the extinction coefficient in $\lambda_{max}$ ($\varepsilon$ = 25700 $M^{-1}\cdot cm^{-1}$).

**Table S 3.** The retention times and UV-vis absorption properties of guests.

| Entry | Retention time (min) | $\lambda_{max}$ (nm) | $\varepsilon$ ($M^{-1}\cdot cm^{-1}$) |
|---|---|---|---|
| i.s. | 8.2 | 277 | 16600 |
| **7a** | 13.1 | 300 | 12300 |
| **7b** | 13.8 | 276 | 42500 |
| **8b** | 12.7 | 276 | 25700 |

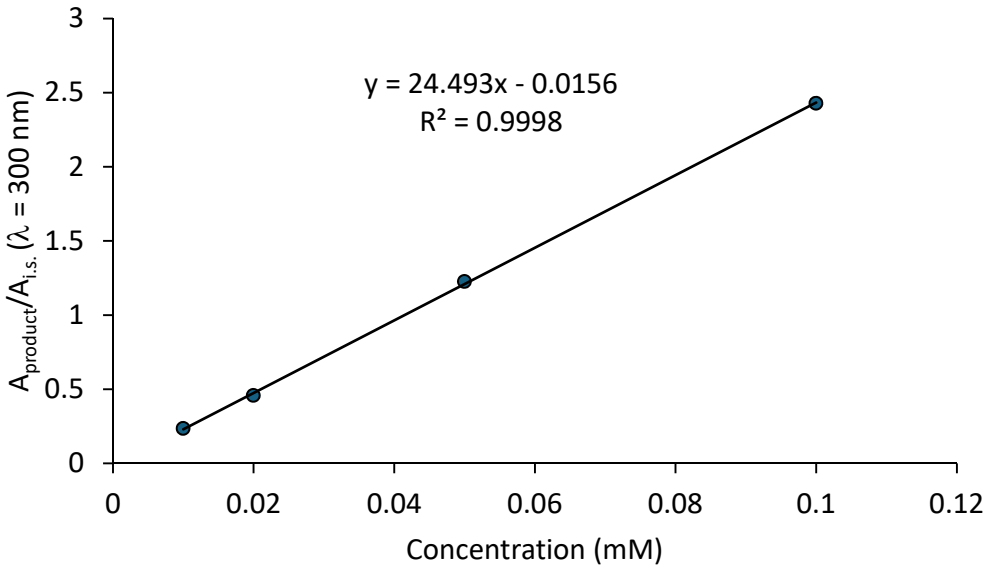


**Figure S 65.** Calibration curve of the 1,4-disubstituted cycloaddition product **7a** using 4-methyl pyridine-*N*-oxide as i.s. (1 mM) and considering ($A_{product}/A_{i.s.}$) ratio at 300 nm.

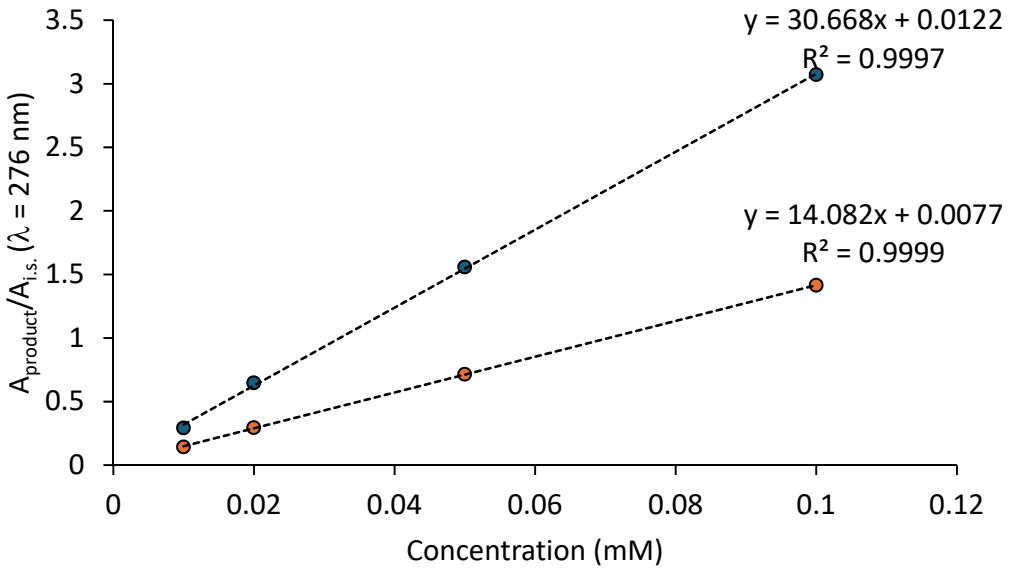


**Figure S 66.** Calibration curve of 1,4- and 1,5- disubstituted cycloaddition products **7b** (green dots) and **8b** (orange dots), respectively using 4-methyl pyridine-*N*-oxide as i.s. (0.1 mM) and considering ($A_{product}/A_{i.s.}$) ratio at 276 nm.

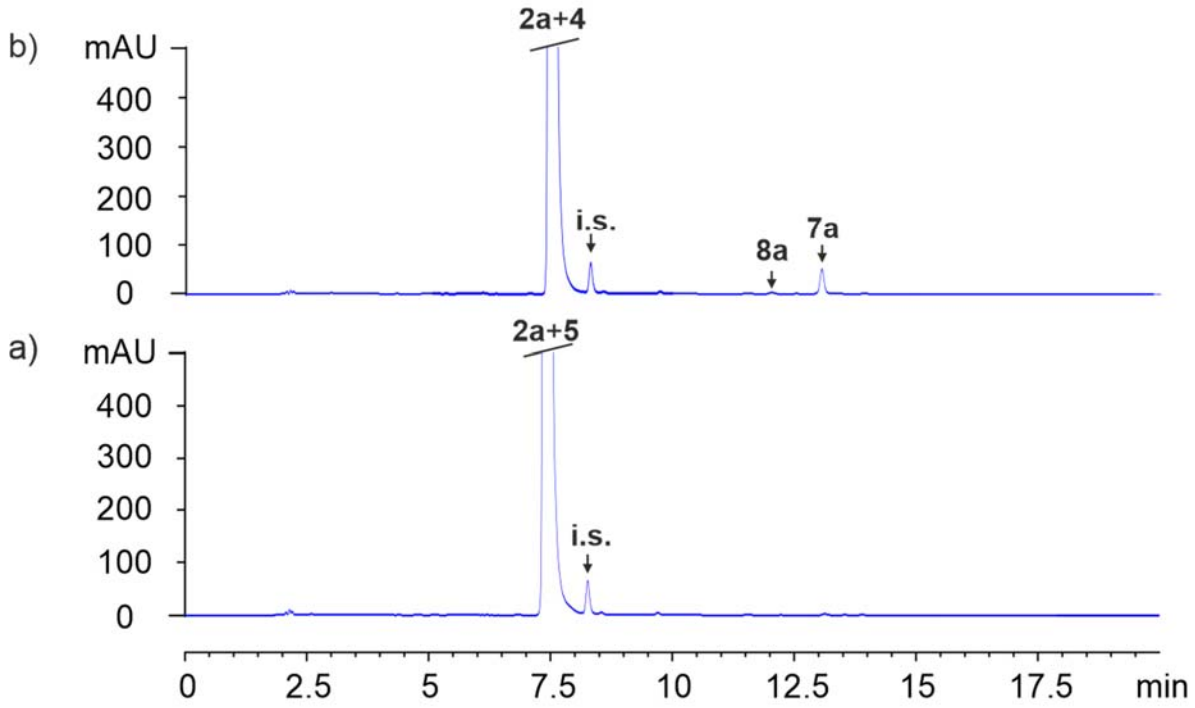


**Figure S 67.** HPLC trace of the reaction crude between **2a** and **4** ($CHCl_3$:$CH_3CN$ 9:1, 25 mM for each and r.t.) a) 0 h and b) 284 h. Both isomers **7a** and **8a** were detected in the reaction mixture. 4-methyl pyridine-*N*-oxide was used as internal standard (i.s.) (1 mM).

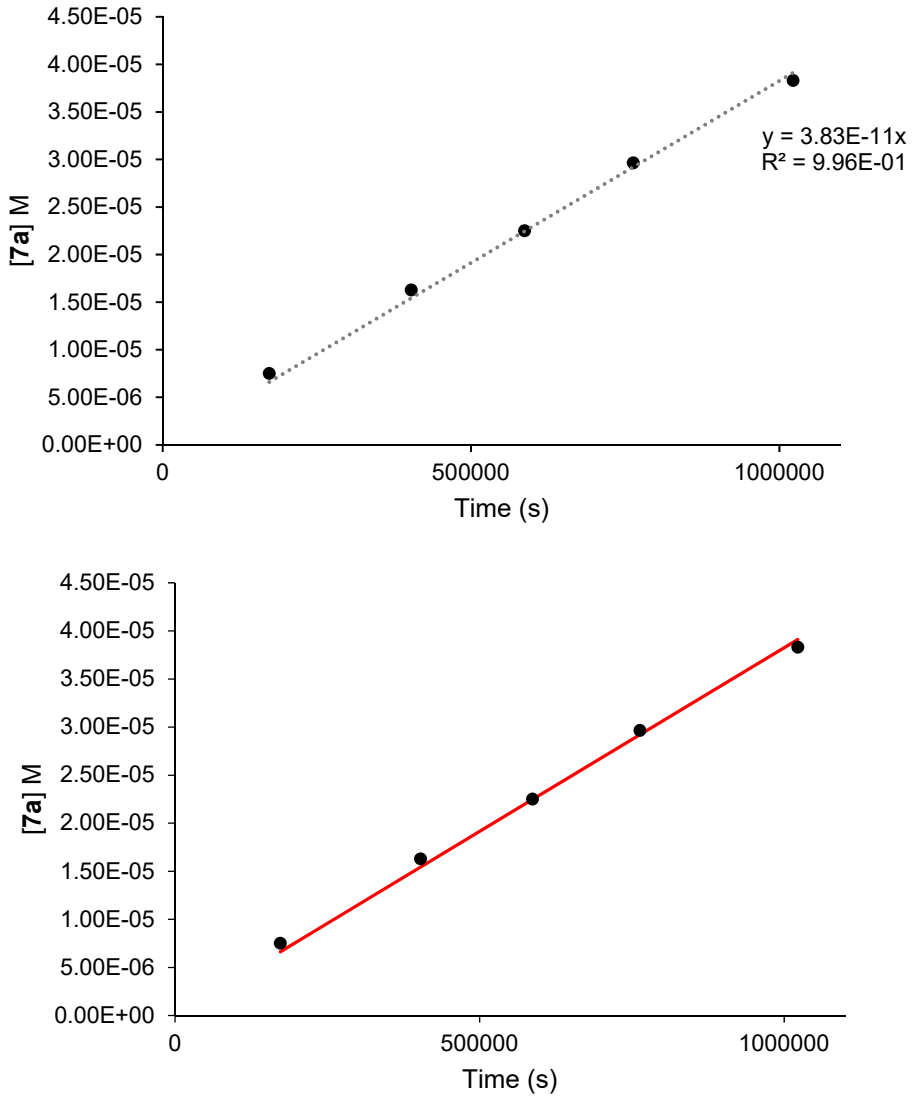


**Figure S 68.** Top) Changes in the concentration of **7a** (black dots) with time (t < 400 h) starting from an equimolar 25 mM mixture of **2a** and **4**, in $CHCl_3$:$CH_3CN$ 9:1. The grey dashed line represents the fit of the experimental kinetic data to a second order irreversible reaction used to determine the initial reaction rate. Bottom) Changes in the concentration of **7a** (black dots) with time (t < 400 h) starting from an equimolar 25 mM mixture of **2a** and **4**, in $CHCl_3$:$CH_3CN$ 9:1. The red solid line represents the best-computer fit of the kinetic experimental data in the bulk using COPASI and a kinetic theoretical model for two competitive irreversible bimolecular reactions yielding the two cycloaddition isomeric products.

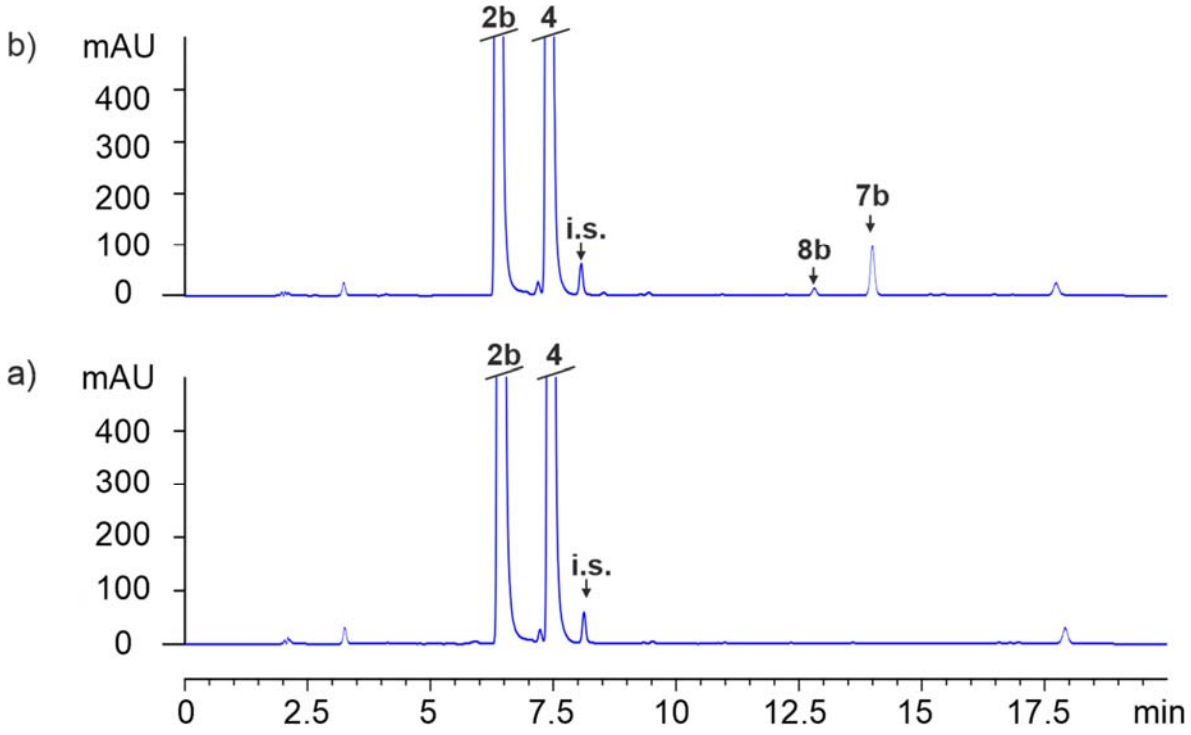


**Figure S 69.** HPLC trace of the reaction crude between **2b** and **4** ($CHCl_3$:$CH_3CN$ 9:1, 25 mM for each and r.t.) a) 0 h and b) 388 h. Both isomers **7b** and **8b** were detected in the reaction mixture. 4-methyl pyridine-*N*-oxide was used as internal standard (i.s.) (0.1 mM).

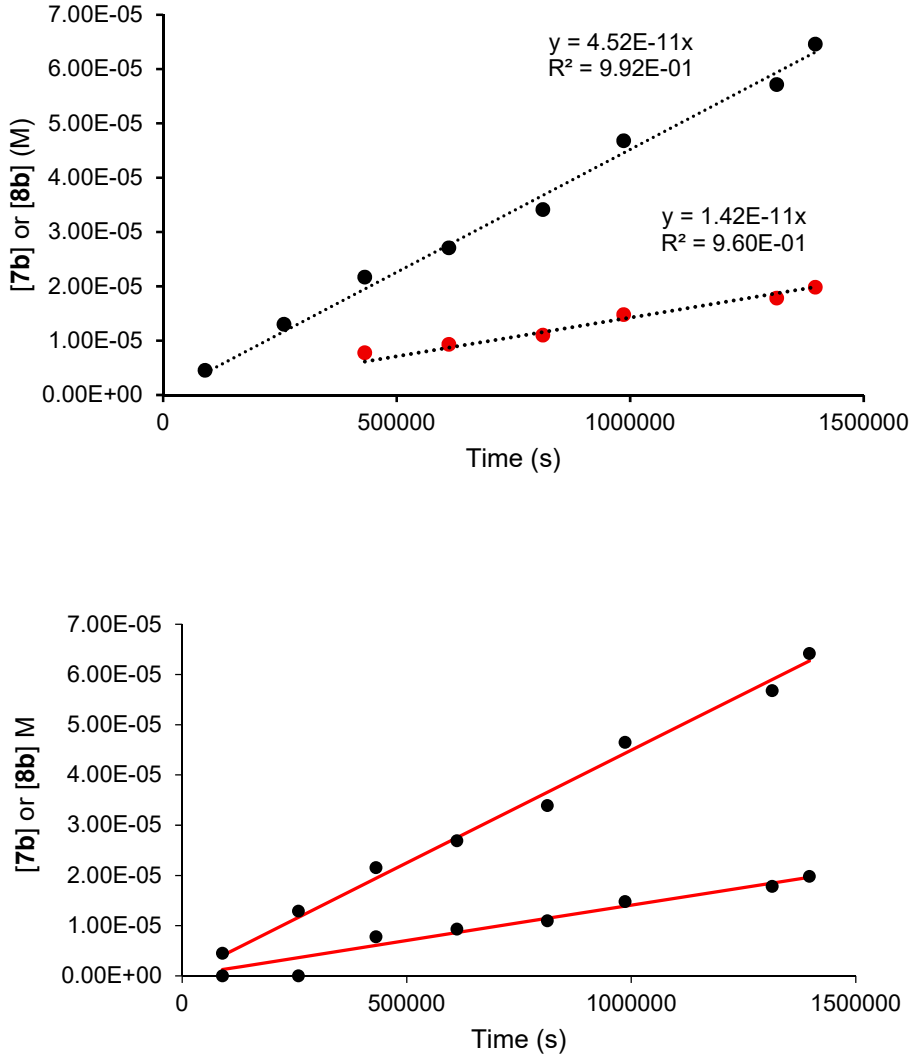


**Figure S 70.** Top) Changes in the concentration of **7b** (black dots) and **8b** (red dots) with time (t < 400 h) starting from an equimolar 25 mM mixture of **2b** and **4**, in $CHCl_3$:$CH_3CN$ 9:1. The dashed grey lines represent the linear fit of the experimental kinetic data to a second order irreversible reaction used to determine the initial reaction rates. Bottom) Changes in the concentration of **7b** and **8b** with time (t < 400 h) starting from an equimolar 25 mM mixture of **2b** and **4**, in $CHCl_3$:$CH_3CN$ 9:1. The red solid line represents the best-computer fit of the kinetic experimental data in the bulk using COPASI and a kinetic theoretical model for two competitive irreversible bimolecular reactions yielding the two cycloaddition isomeric products.

**Table S 4**. Summary of rate constants and initial reaction rates (at 25 mM) and rate constants of the formation of 1,4- and 1,5-disubstituted 1,2,3-triazole isomers **7a**, **7b** and **8b**.

| | $v_0$ ($M \cdot s^{-1}$) [a] | $k_{bulk}' = v_0 / (25 \times 10^{-3})^2$ ($M^{-1} \cdot s^{-1}$)[b] | $k_{bulk}$ ($M^{-1}s^{-1}$) [c] |
|---|---|---|---|
| **7a** | $3.83 \times 10^{-11}$ | $6.13 \times 10^{-8}$ | $6.14 \times 10^{-8}$ |
| **7b** | $4.49 \times 10^{-11}$ | $7.18 \times 10^{-8}$ | $7.20 \times 10^{-8}$ |
| **8b** | $1.42 \times 10^{-11}$ | $2.27 \times 10^{-8}$ | $2.26 \times 10^{-8}$ |
| **8c** | n.d. | n.d. | n.d. |

n.d. not determined. [a] Initial rate calculated from the linear fit of the experimental kinetic data to a second order irreversible reaction. [b] Rate constant values derived from the calculated initial rates. [c] Rate constant values determined by best-computer fit of the kinetic experimental data in the bulk using COPASI and a kinetic theoretical model for two competitive irreversible bimolecular reactions yielding the two cycloaddition isomeric products.

### 4.3. Determination of Activation Parameters

We conducted the AAC reactions between **2b** and **4** at 298 K, 303 K, and 308 K, both in the presence of cage **1** and in its absence. We determined the rate constant at each temperature both in the presence and absence of cage **1**, and we plotted ln(k/T) versus 1/T (Eyring plot), fit the data to the Eyring equation (eq. 1), and derived the corresponding activation enthalpy and entropy.

$$ln\frac{k}{T} = \frac{-\Delta H^{\ddagger}}{R} \cdot \frac{1}{T} + \frac{\Delta S^{\ddagger}}{R} + ln\frac{k_B}{h} \qquad (eq.1)$$

In bulk, we monitored the changes in the concentration of the **7b** and **8b** over time by HPLC. We used 25 mM equimolar mixtures of **2b** and **4** at three different temperatures (296 K, 303 K, and 308 K). We used 4-methylpyridine-*N*-oxide as the internal standard (is). Using the initial rates method, we determined the initial reaction rate producing **7b** and **8b** by linear regression at each temperature. Considering that the cycloaddition reaction was first order for the two reactants, we determined the rate constant value to be $k$(**7b**-bulk) = $v_{0(7b\text{-}bulk)} / (0.025)^2$ and $k$(**8b**-bulk) = $v_{0(8b\text{-}bulk)} / (0.025)^2$. The crude reaction was analyzed by HPLC using XBridge Hilic column and a gradient of $CH_3CN/H_2O$ as eluent (from 98:2 up to 60:40 in 15 min). The initial rates were calculated from the integration of chromatogram peaks of the newly formed species **7b** and **8b** at different times.

For the reaction mediated by cage **1**, we monitored the changes in the concentration of the complex **8b⊂1** over time by $^1$H NMR spectroscopy at three different temperatures (298 K, 303 K and 308 K). Using the initial rates method, we determined the initial reaction rate producing **8b⊂1** by linear regression. Considering that the cycloaddition reaction was first order for the ternary complex, we determined the rate constant value to be $k$(**8b⊂1**) = $v_{0(\mathbf{8b\subset 1})} / 0.004$.

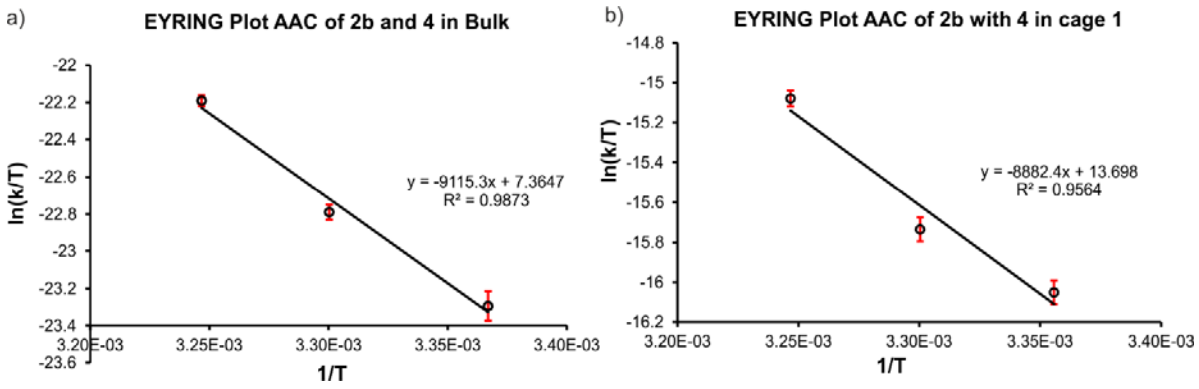


**Figure S 71.** Eyring plots for the AAC between **2b** and **4** in the bulk $CHCl_3$:$CH_3CN$ 9:1 (25 mM) and in cage **1** (**1:2b:4** 1:1:1, 2 mM) in $CDCl_3$:$CD_3CN$ 9:1 to produce **8b** and **8b⊂1**, respectively. Error bars are standard deviations of duplicates.

**Table S 5.** Activation parameters ($\Delta H^{\neq}$, $\Delta S^{\neq}$, $T\Delta S^{\neq}$ (298 K), and $\Delta G^{\neq}$ (298 K)) for the AAC reaction of **2b** and **4** occurring in the bulk and included in cage **1,** producing **8b** and **8b⊂1**, respectively.

| | $\Delta H^{\neq}$ [kcal mol$^{-1}$] | $\Delta S^{\neq}$ [cal mol$^{-1}$ K$^{-1}$] | $T\Delta S^{\neq}$ [kcal mol$^{-1}$] | $\Delta G^{\neq}$ [kcal mol$^{-1}$] |
|---|---|---|---|---|
| Bulk | 16.3 (±0.5) | -38.4 (±0.5) | -11.4 (±0.5) | 27.8 (±0.5) |
| Cage **1** | 17.7 (±1.8) | -19.9 (±0.6) | -5.9 (±1.8) | 23.5 (±2.5) |

### 4.4. Selected computational studies

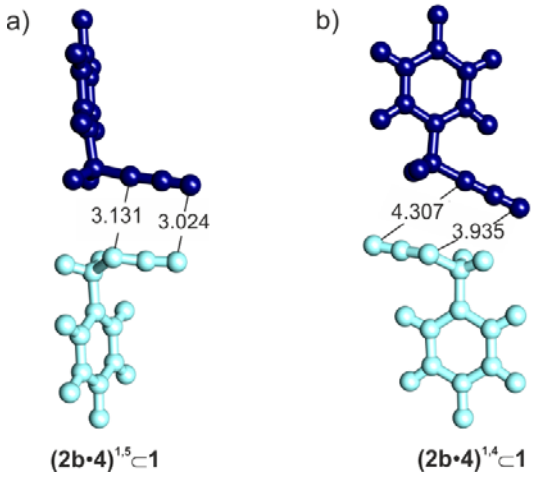


**Figure S 72.** Distances between the carbon and nitrogen atoms of the dipolarophile (alkyne **4**) and the 1,3-dipole (azide **2b**) in the energy-minimized structures of the two conformers of the ternary complexes, (**2b•4**)$^{1,5}$⊂**1** (a), and (**2b•4**)$^{1,4}$⊂**1** (b), respectively.

## 5. References

[1] Y. Li, C. F. M. Mirabella, G. Aragay and P. Ballester, Acceleration and Selectivity of 1,3-Dipolar Cycloaddition Reactions Included in a Polar [4 + 2] Octa-imine Bis-calix[4]pyrrole Cage, *JACS Au*, 2025, **5**, 902-912.
[2] Q.-Y. Yang and J.-M. Lehn, Bright White-Light Emission from a Single Organic Compound in the Solid State, *Angew. Chem., Int. Ed.*, 2014, **53**, 4572-4577.